

# Journal Pre-proof

Design, synthesis and 3D-QSAR analysis of novel thiopyranopyrimidine derivatives as potential antitumor agents inhibiting A549 and Hela cancer cells

Bingbing Zhao, Chengwu Zhao, Xiaohan Hu, Shan Xu, Zhou Lan, Yuping Guo, Zunhua Yang, Wufu Zhu, Pengwu Zheng



PII: S0223-5234(19)30961-4

DOI: <https://doi.org/10.1016/j.ejmech.2019.111809>

Reference: EJMECH 111809

To appear in: *European Journal of Medicinal Chemistry*

Received Date: 16 July 2019

Revised Date: 17 September 2019

Accepted Date: 21 October 2019

Please cite this article as: B. Zhao, C. Zhao, X. Hu, S. Xu, Z. Lan, Y. Guo, Z. Yang, W. Zhu, P. Zheng, Design, synthesis and 3D-QSAR analysis of novel thiopyranopyrimidine derivatives as potential antitumor agents inhibiting A549 and Hela cancer cells, *European Journal of Medicinal Chemistry* (2019), doi: <https://doi.org/10.1016/j.ejmech.2019.111809>.

This is a PDF file of an article that has undergone enhancements after acceptance, such as the addition of a cover page and metadata, and formatting for readability, but it is not yet the definitive version of record. This version will undergo additional copyediting, typesetting and review before it is published in its final form, but we are providing this version to give early visibility of the article. Please note that, during the production process, errors may be discovered which could affect the content, and all legal disclaimers that apply to the journal pertain.

© 2019 Published by Elsevier Masson SAS.

**Design, synthesis and 3D-QSAR analysis of novel thiopyranopyrimidine derivatives as potential antitumor agents inhibiting A549 and Hela cancer cells**

Bingbing Zhao<sup>a,b,#</sup>, Chengwu Zhao<sup>c,#</sup>, Xiaohan Hu<sup>a</sup>, Shan Xu<sup>a,\*</sup>, Zhou Lan<sup>a</sup>, Yuping Guo<sup>a</sup>, Zunhua Yang<sup>b</sup>, Wufu Zhu<sup>a,\*</sup>, Pengwu Zheng<sup>a,\*</sup>

<sup>a</sup>*Jiangxi Provincial Key Laboratory of Drug Design and Evaluation, School of Pharmacy, Jiangxi Science & Technology Normal University, 605 Fenglin Road, Nanchang, Jiangxi 330013, China*

<sup>b</sup>*College of Pharmacy, Jiangxi University of Traditional Chinese Medicine, Nanchang 330004, China,*

<sup>c</sup>*Department of Sports Medicine, The First Hospital of Jilin University, 71 Xinmin Road, Changchun, Jilin 130021, China*

**Abstract:**

Four series of thiopyranopyrimidine AZD9291 derivatives containing acrylamide structure were designed, synthesized and evaluated for their antiproliferative activity against A549 and Hela cancer cells. Most of the compounds exhibited excellent antiproliferative activity against A549 cells. Moreover, the compounds with indole ring fluorine substituted exhibited better antiproliferative activity against Hela cells. The most promising compound **23g** exhibited excellent enzymatic inhibitory activity and selectivity for EGFR<sup>L858R/T790M</sup> double mutations. The IC<sub>50</sub> value against EGFR<sup>L858R/T790M</sup> kinase was 16 nM. The compound **23g** inhibits selectively against the mutated form of EGFR, with the selectivity more than 125-fold. Furthermore, compound **23g** also inhibited A549 cells, Hela cells and H1975 cells proliferation at a low concentration, and the IC<sub>50</sub> values were 0.057 μM, 0.104 μM and 0.916 μM, respectively. To further investigate the QSARs of thiopyranopyrimidine derivatives, the CoMFA ( $q^2 = 0.765$ ,  $r^2 = 0.965$ ) and CoMSIA ( $q^2 = 0.875$ ,  $r^2 = 0.956$ ) models on Hela cancer cells were established. The generated 3D-QSAR model was validated to be reliable and can be used for further design and optimization of novel and selective EGFR inhibitors.

**Keywords:** Thiopyranopyrimidine; EGFR; inhibitor; 3D-QSAR; CoMFA; CoMSIA

## 1. Introduction

Epidermal growth factor receptor (EGFR) is widely expressed in most human cells and plays a vital role in maintaining normal life activities<sup>1-3</sup>. Ras-Raf-MARK signaling pathway, PI3K/Akt/mTOR signaling pathway and JAK-STAT

---

\*Corresponding authors.

E-mail: zhengpw@126.com (P. Zheng), zhuwufu-1122@163.com (W. Zhu), shanxu9891@126.com (S. Xu);

#These authors made equal contributions to this work.

signaling pathway are the main EGFR downstream signaling pathways reported in the literatures<sup>4,5</sup>. These signaling pathways coordinate with each other and jointly control a series of life activities such as cell survival, proliferation and differentiation<sup>6,7</sup>. It was reported by the World Health Organization (WHO) that the incidence of overexpression or mutation of EGFR signaling pathway in lung cancer, cervical cancer, breast cancer and other malignant tumor cells was as high as 80%<sup>8</sup>. Consequently, deregulation or mutation of EGFR signaling pathway will lead to the occurrence of diseases or malignancy.

Lung cancer ranks the first place in the world's total cancer mortality rate. The annual incidence of lung cancer is as high as 1.8 million and the death toll is close to 1.6 million<sup>9,10</sup>. More than 85% of lung cancer patients belong to non-small cell lung cancer (NSCLC) sub-types, with a 5-year survival rate of less than 10%<sup>11-13</sup>. The researches have shown that the EGFR kinase mutations were the leading cause of NSCLC, for example, the T790M mutation<sup>14</sup>, L858R mutation<sup>15</sup>, C797S mutation<sup>16</sup> and other mutations<sup>17</sup>. In the past decades, a number of EGFR-target kinase inhibitors (**1**, Gefitinib; **2**, Afatinib and **3**, AZD9291) have been approved by Food and Drug Administration (FDA) for treatment of EGFR mutations in NSCLC patients<sup>18-20</sup>. As the first FDA-approved third-generation irreversible EGFR inhibitor, AZD9291 has high selectivity for EGFR<sup>T790M</sup> mutation and remains the most widely used medicine for clinical treatment of EGFR<sup>T790M</sup> mutation and advanced metastatic NSCLC<sup>21,22</sup>. However, the clinical therapeutic effect of AZD9291 is not satisfactory. Some patients developed drug-resistant mutation (C797S) and serious side effects (cardiotoxicity, diarrhea and rash) after treated with AZD9291<sup>22</sup>.

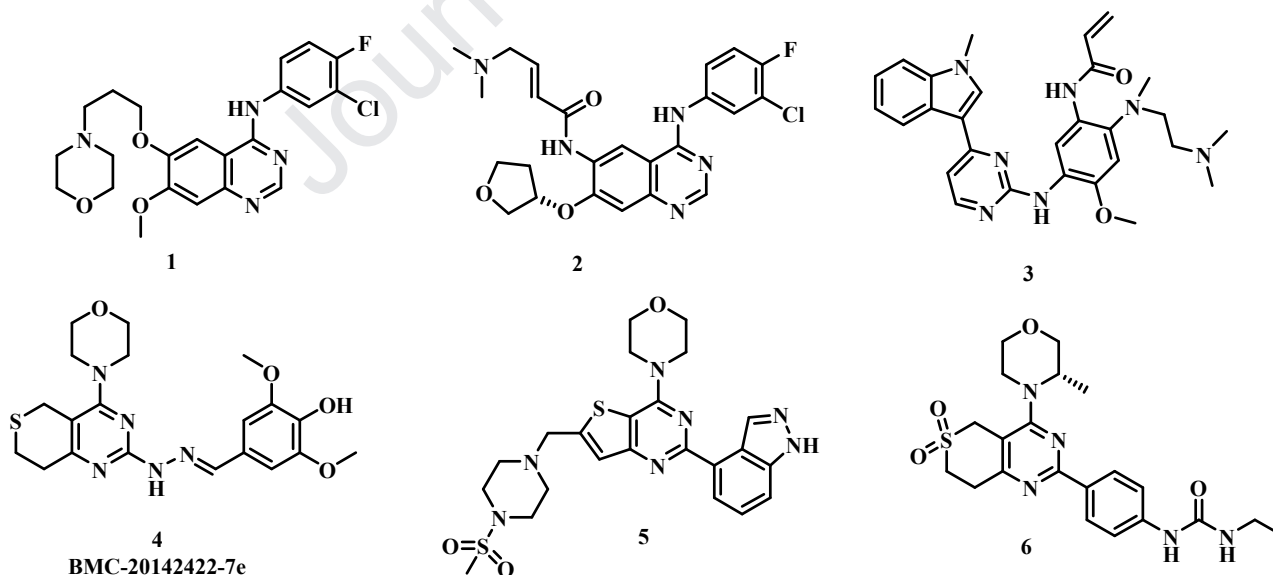


**Figure 1** Representative EGFR inhibitors (**1–3**) and PI3k/mTOR inhibitors (**4–6**).

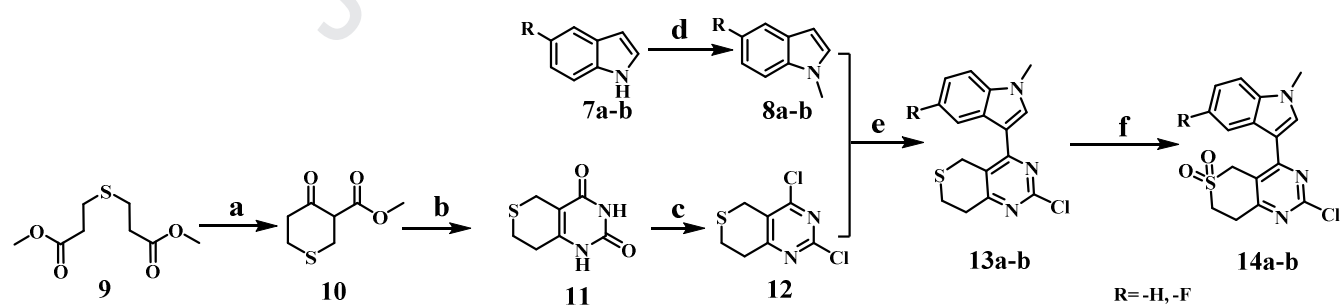
However, in addition to lung cancer, cervical cancer is also the cancer with the highest mortality in the world, accounting for 33% of the total number of female cancer deaths, and more than 100,000 women die of cervical cancer every year worldwide<sup>23</sup>. There is no effective medicine can cure cervical cancer completely. Human papillomavirus (HPV) vaccine is the most effective vaccine for preventing cervical carcinoma at present<sup>24</sup>. But it still has many safety

problems (skin allergy and peripheral neuropathy). The disorder in PI3K/mTOR signal pathway was considered to be the main cause of cervical cancer<sup>25</sup>. In recent years, many pyrimidine heterocyclic derivatives were reported as PI3K-Akt-mTOR signal pathway inhibitors (**4** BMC-20142422-7e, **5**, **6**)<sup>26-28</sup>. The compound **5** (GDC0941) and compound **6** (PF-05139962) were effective PI3K signaling pathway inhibitors, which can significantly inhibit the growth of cervical cancer cells (Hela). The IC<sub>50</sub> values of compound **5** and **6** against PI3K kinase were 3 nM and 5 μM, respectively<sup>27,28</sup>. The compound **4** (BMC-20142422-7e) had a good inhibitory ability on mTOR kinase, with the IC<sub>50</sub> value of 0.27 μM<sup>26</sup>. These inhibitors have achieved remarkable efficiency in pre-clinical trials and are currently being studied in the clinical trial. Consequently, the development of EGFR inhibitors based on EGFR signaling pathways will greatly improve the accuracy of drug design and shorten the drug development of period.

In this research, the structure-based drug design (SBDD) strategy was applied to further study the structure-activity relationship of lead compounds. Based on the structures of the reported potent leading compounds, aliphatic heterocycles were introduced into pyrimidine ring by expansion principle and combination principle. Finally, four series of thiopyranopyrimidine derivatives containing acrylamide structure (**21a-g**, **22a-g**, **23a-g** and **24a-g**) were designed and synthesized. It is desirable to obtain EGFR inhibitors with highly selectivity and potent inhibitory activities against EGFR<sup>T790M</sup> mutant kinase. In addition, it is also expected to obtain inhibitors with dual cancer cells inhibitory activities of A549 cancer cells and Hela cancer cells.

## 2. Results and discussion

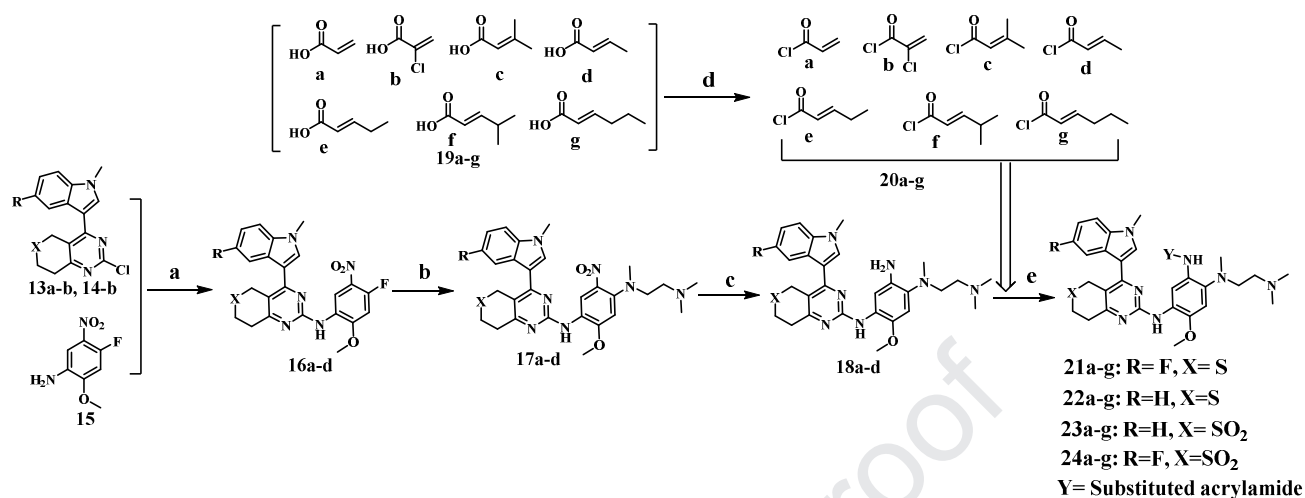
### 2.1. Chemistry



**Scheme 1** Synthetic routes of the compounds **13a-b** and **14a-b**. Reagents and conditions: (a) NaH, THF, rt., 2 h; (b) Urea, C<sub>2</sub>H<sub>5</sub>ONa, C<sub>2</sub>H<sub>5</sub>OH, 70 °C, 2.5 h; (c) POCl<sub>3</sub>, 100 °C, 3 h; (d) CH<sub>3</sub>I, NaH, THF, rt., 1.5 h; (e) AlCl<sub>3</sub>, DME, 80 °C, 3 h; (f) Na<sub>2</sub>WO<sub>4</sub>·2H<sub>2</sub>O, H<sub>2</sub>O<sub>2</sub>, THF, rt., 0.5 h.

The synthetic routes of the compounds **13a-b** and **14a-b** were shown in **Scheme 1**. Commercially available starting material 5-fluorindole **7a** or indole **7b** reacted with iodomethane to get **8a-b**. **10** was obtained by the reaction of

self-ester condensation from commercially available **9**. Next, **10** cyclized with urea to obtain **11**. Then, **11** reacted with phosphorus oxychloride to obtain intermediate **12**. Intermediate **12** and **8a-b** undergone Friedel-Crafts alkylation reaction to obtain intermediate **13a-b**. **14a-b** were obtained by the reaction of oxidation from **13a-b**.



**Scheme 2** Synthetic routes of the compounds **21a-g**, **22a-g**, **23a-g** and **24a-g**. Reagents and conditions: (a) TsOH, 1,4-dioxane, 85 °C, 3 h; (b) N,N,N'-trimethylethylenediamine, DIPEA, DMA, 110 °C, 2.5 h; (c) Zn, NH<sub>4</sub>Cl, C<sub>2</sub>H<sub>5</sub>OH, H<sub>2</sub>O, 105 °C, 3 h; (d) Oxalyl chloride, DMF, DCM, 0 °C, 0.5 h; (e) NaHCO<sub>3</sub>, DCM, 0 °C, 0.5-2 h.

The synthetic routes of the compounds **21a-g**, **22a-g**, **23a-g** and **24a-g** were shown in **Scheme 2**. The starting material 4-fluoro-2-methoxy-5-nitroaniline **15** reacted with intermediates **13a-b** and **14a-b** to get **16a-d**. **18a-d** were got by the reaction of reduction from **17a-d** with **16a-d** as raw materials. Different substituted acid chloride (**20a-g**) were got from the corresponding acrylic acids (**19a-g**) by the reaction of chlorination. Finally, **20a-g** reacted with **18a-d** to obtain the target compounds **21a-g**, **22a-g**, **23a-g** and **24a-g**.

## 2.2. Docking study of lead compounds

The *silico* molecular docking strategy was applied to study the binding modes between compound skeletons and receptor proteins. Sybyl 8.1 software (Tripos Associates Inc., USA) was used to simulate the binding patterns of lead compounds AZD9291 and BMC-20142422-7e<sup>27</sup> (**4**, **Figure 1**) with EGFR<sup>T790M</sup> protein (PDB code: 3IKA, www.rcsb.org). The Surflex-Dock Geom was used to optimize the docking model results. Only the model with the best CS score was selected to generate protein-ligand complexes for further molecular docking research. As depicted in **Figure 2**, the whole AZD9291 skeleton embedded into hydrophobic pocket of EGFR<sup>T790M</sup> protein with a “U-shape” structure (**Figure 2C**) and closely combined with EGFR<sup>T790M</sup> protein. The pyrimidine ring was far away from gatekeeper residue Met790. The pyrimidine ring and the amino bridge formed a bidentate hydrogen bond with hinge region residue Met793. The acrylamide side chain extended to the conserved region residue Cys797 and formed a hydrogen bond with residue Cys797. As illustrated in the **Figure 2B**, the compound BMC-20142422-7e also combined well with EGFR<sup>T790M</sup> protein

and formed a strong bidentate hydrogen bond with hinge region residue Met793. The phenolic hydroxyl structure extended to the conserved residue Cys797, but without hydrogen bond formed. The orientation of the whole molecular skeleton of BMC-20142422-7e in the EGFR protein cavity was basically the same as that of AZD9291(**Figure 2D**), and the thiopyranopyrimidine ring also formed hydrogen bonding forces with EGFR protein. The molecular simulation results further indicated that the thiopyranopyrimidine structure can be used to design novel EGFR inhibitors.

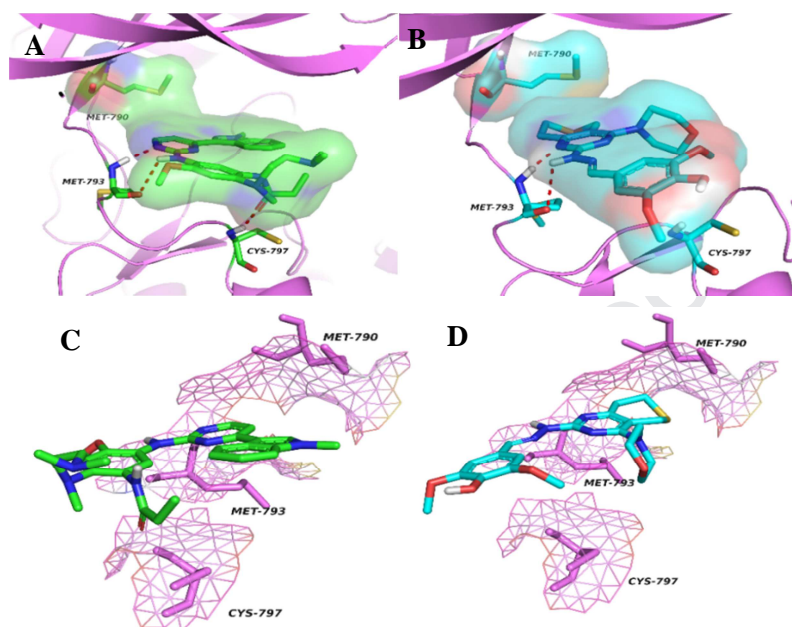


**Figure 2** Binding site of leading compounds. (A) The docking result of AZD9291 (green) bound to EGFR<sup>T790M</sup> protein (PDB code:3IKA). (B) The docking result of BMC-20142422-7e (cyan) bound to EGFR<sup>T790M</sup> protein. (C) The spatial orientation of AZD9291 (green) bound to EGFR<sup>T790M</sup> protein. (D) The spatial orientation of BMC-20142422-7e (cyan) bound to EGFR<sup>T790M</sup> protein.

### 2.3 Structure-based drug design strategy

First of all, we conducted the computer simulation docking of the leading compounds. According to the docking results (**Figure 2**), we can know that the pyrimidine ring of AZD9291 and the thiopyranopyrimidine ring of BMC-20142422-7e all formed a bidentate hydrogen bond with the hinge region residue Met793 of EGFR<sup>T790M</sup> protein. It was clearly that any modifications to the structures of those two parts will change the biological activity of the target compounds. The thiopyranopyrimidine structure of PI3K/mTOR inhibitor BMC-20142422-7e formed a bidentate hydrogen bond with EGFR<sup>T790M</sup> protein, which inspired us to firstly introduce aliphatic heterocycle into pyrimidine ring of AZD9291. Through this strategy, the space volume of pyrimidine ring could be further expanded to fully occupy the protein cavity. In addition, it is possible to retain the PI3K/mTOR kinase inhibitory activity of thiopyranopyrimidine skeleton. Secondly, the halogen and small molecular alkyl side chains were introduced in the ortho position of acrylamide side chain of AZD9291 to weaken the covalent binding ability of the target compounds to non-target proteins. In this way, the

cytotoxicity and side effects of the target compound will be greatly reduced. Finally, the electron-withdrawing group F-atom was introduced into indole ring to change the electron cloud distribution of the indole ring and improve the overall physical and chemical properties of the compound. Thus, it is hopeful to discover novel inhibitors with selectivity and potent inhibition over EGFR<sup>T790M</sup> protein, and also expect to discover inhibitors with dual cancer cells inhibitory activities.

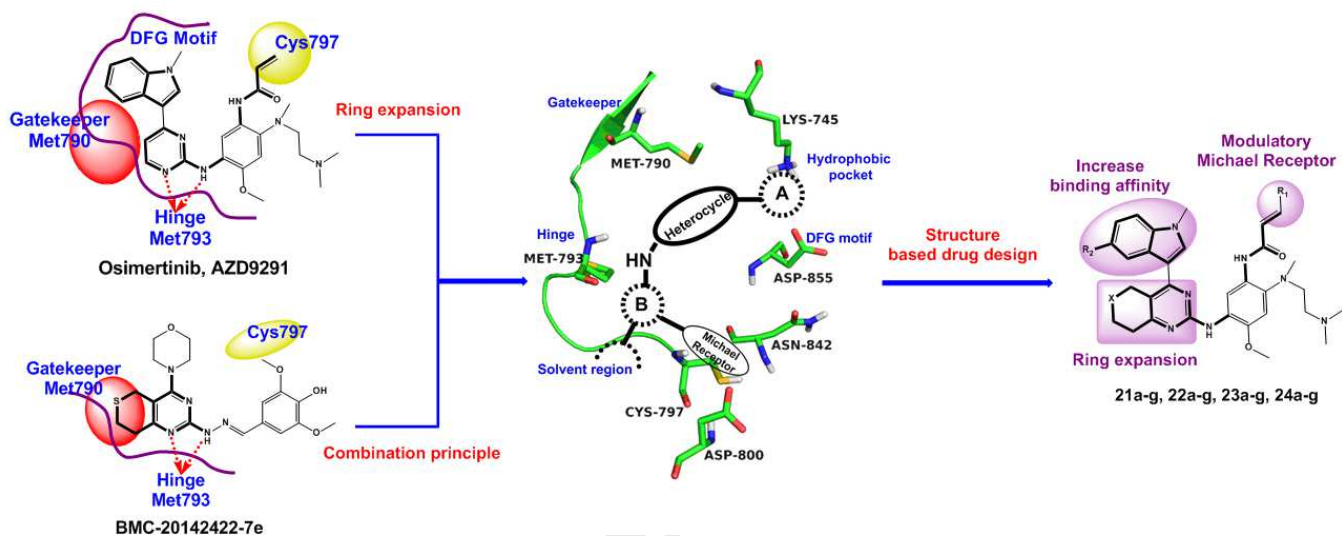


**Figure 3** Structure based drug design strategy from chemical structures of lead compounds.

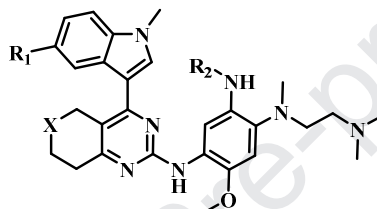
## 2.4. Biological evaluation

### 2.4.1. *In vitro* antiproliferative activity against A549 and Hela cells

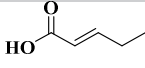
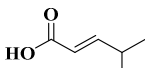
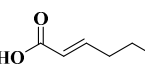
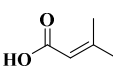
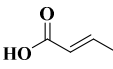
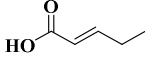
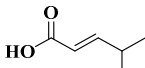
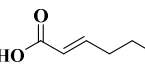
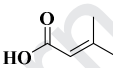
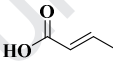
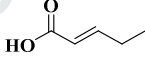
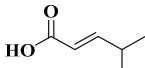
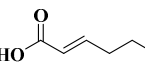
The *in vitro* antiproliferation activity of compounds **21a-g**, **22a-g**, **23a-g** and **24a-g** were shown in **Table 1**. As expected, most of the thiopyranopyrimidine derivatives retained the excellently antiproliferative activity against A549 cells with the  $IC_{50}$  values range from 0.057  $\mu$ M to 7.568  $\mu$ M. To our surprise, the majority of thiopyranopyrimidine derivatives also exhibited potent antiproliferation activity against Hela cells, especially compounds with 5-fluoroindole structure (the  $IC_{50}$  values of compounds against Hela cells range from 0.175  $\mu$ M to 7.096  $\mu$ M). In general, compounds containing 5-fluoroindole structure (**21a-g** and **24a-g**) had a higher antiproliferative activity against Hela cells than that of compounds (**22a-g** and **23a-g**) without fluorine-substituted indole ring structure. Furthermore, compounds (**23a-g** and **24a-g**) containing a thiopyran dioxides ring structure (the  $LogD_{7,4}$  values range from 1.8 to 3.1) had a better  $LogD_{7,4}$  value than that of compounds (**21a-g** and **22a-g**) without thiopyran ring double oxidated (the  $LogD_{7,4}$  values range from 3.8 to 5.2). However, the antiproliferative activity show that the double oxidation strategy had little effect on the antiproliferative activity of the target compound. As the volume of acrylamide side chain increase, the antiproliferative activity of the target compounds against A549 cells gradually increased. But the antiproliferative activity of the target compounds against Hela cells remained unchange or even decrease slightly. The introduction of Cl-atom on the

acrylamide was beneficial to increase the antiproliferative activity of the target compound against A549 cells. The  $IC_{50}$  values of compounds **21a**, **22a**, **23a** and **24a** against A549 cells were 4.545  $\mu$ M, 0.506  $\mu$ M, 8.685  $\mu$ M and 4.635  $\mu$ M, respectively. And the  $IC_{50}$  values of chlorine substituted compounds **21b**, **22b**, **23b** and **24b** against A549 cells were 0.864  $\mu$ M, 0.716  $\mu$ M, 0.881  $\mu$ M and 3.183  $\mu$ M, respectively. However, as shown in **Table1**, the introduction of Cl-atoms was not conducive to increase the biological activity of the compounds against Hela cells and the antiproliferative activities of compounds **21b**, **22b**, **23b** and **24b** against Hela cells were weaker than that of compounds **21a**, **22a**, **23a** and **24a**. The preferred compounds **23b** (the  $IC_{50}$  values against A549 and Hela cells were 0.881  $\mu$ M and 0.205  $\mu$ M) and **23g** (the  $IC_{50}$  values against A549 and Hela cells were 0.057  $\mu$ M and 0.104  $\mu$ M) both exhibited an excellent dual antiproliferative activity against A549 and Hela cells.

**Table 1** The antiproliferative activities of compounds **21a-g**, **22a-g**, **23a-g** and **24a-g**.



Compd.	R <sub>1</sub>	R <sub>2</sub>	X	Cellular activity $IC_{50}$ ( $\mu$ M) <sup>a</sup>		LogD <sub>7.4</sub> <sup>b</sup>
				A549	Hela	
<b>21a</b>	F		S	4.545	0.728	4.0
<b>21b</b>	F		S	0.864	0.980	4.2
<b>21c</b>	F		S	0.902	0.284	4.3
<b>21d</b>	F		S	5.312	0.275	4.6
<b>21e</b>	F		S	1.451	0.839	4.8
<b>21f</b>	F		S	1.154	1.327	5.1
<b>21g</b>	F		S	5.187	0.966	5.2
<b>22a</b>	H		S	0.506	1.297	3.8
<b>22b</b>	H		S	0.716	1.005	4.3
<b>22c</b>	H		S	0.583	2.361	4.2
<b>22d</b>	H		S	6.863	1.648	4.5

<b>22e</b>	H		S	0.236	0.799	4.6
<b>22f</b>	H		S	0.788	0.711	4.9
<b>22g</b>	H		S	0.571	0.652	5.1
<b>23a</b>	H		SO <sub>2</sub>	8.685	0.115	1.8
<b>23b</b>	H		SO <sub>2</sub>	0.881	0.205	2.2
<b>23c</b>	H		SO <sub>2</sub>	0.787	4.519	2.2
<b>23d</b>	H		SO <sub>2</sub>	4.257	6.011	2.5
<b>23e</b>	H		SO <sub>2</sub>	1.351	5.224	2.7
<b>23f</b>	H		SO <sub>2</sub>	0.038	2.964	2.9
<b>23g</b>	H		SO <sub>2</sub>	0.057	0.104	2.6
<b>24a</b>	F		SO <sub>2</sub>	4.635	0.175	2.0
<b>24b</b>	F		SO <sub>2</sub>	3.183	2.931	2.4
<b>24c</b>	F		SO <sub>2</sub>	2.138	5.916	2.4
<b>24d</b>	F		SO <sub>2</sub>	3.986	2.471	2.6
<b>24e</b>	F		SO <sub>2</sub>	5.832	7.096	2.8
<b>24f</b>	F		SO <sub>2</sub>	3.754	0.261	3.1
<b>24g</b>	F		SO <sub>2</sub>	7.568	2.333	3.3
<b>AZD9291<sup>c</sup></b>	-	-	-	0.462	0.975	3.0

<sup>a</sup>The values are an average of two separate determinations;

<sup>b</sup>LogD<sub>7,4</sub> values were calculated online on the chemaxon website (www.chemaxon.com);

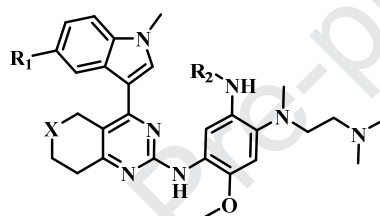
<sup>c</sup>Used as a positive control.

#### 2.4.2. *In vitro* EGFR kinase ELISA assay

Based on the results of cellular antiproliferative activities of the target compounds, a partial representative compounds were selected to test for EGFR kinase activity. The EGFR enzymatic activities of representative compounds were shown in **Table 2**. Most of the tested compounds showed potent EGFR<sup>T790M</sup> kinase inhibitory activity and weak EGFR<sup>WT</sup> kinase inhibitory ability. In particular, compounds **22a**, **22b**, **23b** and **23g** showed excellent EGFR<sup>T790M</sup> mutant kinase inhibitory

activity. Their  $IC_{50}$  values over EGFR<sup>T790M</sup> mutant kinase were 35 nM, 31 nM, 990 nM and 16 nM, respectively. The compounds with indole ring unsubstituted (**22a**, **22b** and **23g**) showed excellent selectivity to EGFR<sup>T790M</sup> mutant kinase. Especially the selectivity of compound **23g** against EGFR<sup>T790M</sup> mutant kinase to EGFR<sup>WT</sup> kinase was more than 125-fold. The compounds **22a**, **22b**, **23b** and **24c** had higher inhibitory activity against EGFR<sup>WT</sup> kinase with the  $IC_{50}$  values of 511 nM, 570 nM, 104 nM and 201 nM, respectively. It indicated that the acrylamide side chain with small volume structures substituted were more beneficial to increase the activity of the compounds on EGFR<sup>WT</sup> kinase, while large volume substituted groups were more beneficial to increase the inhibitory activity of the compound on EGFR<sup>T790M</sup> kinase. Consequently, the results of cellular antiproliferative activity and kinase activity indicated that compounds **22b** and **23g** had the excellent dual antiproliferative activity of A549 and Hela cells and EGFR<sup>T790M</sup> mutant kinase inhibitory ability, which can be used as potential EGFR inhibitors for further research.

**Table 2** The EGFR enzymatic activities of representative compounds.



Compd.	EGFR $IC_{50}$ (nM) <sup>a</sup>		Selectivity (WT/TL)
	WT <sup>b</sup>	TL <sup>c</sup>	
<b>21e</b>	>2000	1128	>1.8
<b>21f</b>	>2000	1689	>1.2
<b>22a</b>	511	35	14.6
<b>22b</b>	570	31	18.4
<b>22e</b>	>2000	1248	>1.6
<b>22f</b>	>2000	1621	>1.2
<b>23b</b>	104	990	1.1
<b>23f</b>	>2000	1753	>1.2
<b>23g</b>	>2000	16	>125
<b>24c</b>	201	>2000	-
<b>AZD9291<sup>d</sup></b>	16	8	2.0

<sup>a</sup> Enzymatic assays were performed by using the ELISA-based EGFR-tyrosine kinase (TK) assay;

<sup>b</sup> Wide type EGFR kinase;

<sup>c</sup> T790M and L858R double mutation EGFR kinase;

<sup>d</sup> Used as a positive control.

#### 2.4.3 *In vitro* antiproliferative activity against H1975 cells

The results of EGFR enzymatic activities of representative compounds inspired us to further investigate the inhibitory

activity of the target compounds on H1975 cells (EGFR<sup>T790M/L858R</sup> double mutation). The in vitro inhibition rates of H1975 cells at 10  $\mu$ M concentration of representative compound were first conducted to explore the the inhibitory ability against H1975 cells. As shown in **Table 3**, all the representative compounds inhibit H1975 cell growth well. Except for compound **22a**, the inhibition rates of other compounds were over 99%. The results indicated that the representative compounds almost completely inhibited the growth of H1975 cells at a concentration of 10  $\mu$ M. Next, we tested the IC<sub>50</sub> value of compound **22b**, **23b** and **23g** in detail with the AZD9291 as a positive control. The most representative compound 23g showed potent inhibitory ability over H1975 cells with the IC<sub>50</sub> value of 0.916  $\mu$ M. The antiproliferation activity results of H1975 cells further indicate that the thiopyranopyrimidine derivative have multiple cell inhibitory activities, which can be used not only as EGFR<sup>T790M/L858R</sup> double mutation inhibitors, but also as potential cervical cancer inhibitors.

**Table 3** The antiproliferative activities of compounds **21f**, **22a**, **22b**, **23b**, **23g** and **24f**.

Compd.	H1975 Cellular activity	
	Inhibition <sup>a</sup>	IC <sub>50</sub> ( $\mu$ M) <sup>b</sup>
<b>21f</b>	99.68 %	-
<b>22a</b>	55.61 %	-
<b>22b</b>	99.56 %	4.211
<b>23b</b>	99.05 %	4.230
<b>23g</b>	99.45 %	0.916
<b>24f</b>	99.44 %	-
<b>AZD9291<sup>c</sup></b>	-	0.073

<sup>a</sup> Inhibition rate of H1975 cells at 10  $\mu$ M concentration;

<sup>b</sup> The values are an average of two separate determinations;

<sup>c</sup> Used as a positive control;

- Means not conduct experiment.

#### 2.4.4 In silico molecular docking study

The molecular docking studies were performed to evaluate the structure-activity relationship between different thiopyranopyrimidine derivatives at the molecular level. As shown in **Figure 4**, compounds **22b**, **23b**, **23g** and **24c** were well embedded in the hydrophobic cavity of the EGFR<sup>T790M</sup> protein and formed multiple hydrogen bonds with the EGFR<sup>T790M</sup> protein. The thiopyranopyrimidine structure of compound **22b** formed a bidentate hydrogen bond with the hinge region residue Met793 of the EGFR<sup>T790M</sup> protein with the hydrogen bond lengths of 1.9 Å and 2.6 Å, respectively. The thiopyran skeleton was far away from the Met790 mutant residue, indicating that the T790M mutation will not impact the combination of the compounds and the EGFR<sup>T790M</sup> protein. Furthermore, the O-atom of the acrylamide side chain also formed a hydrogen bond with the conservative region residue Cys797. The hydrogen bond length was 1.8 Å.

The binding modes of compounds **23b** and **24c** to EGFR<sup>T790M</sup> protein were similar to the compound **22c**, and the difference was that the ethanediamine side chain of compound **23b** formed a weaker hydrogen bond with residue Leu718 with the hydrogen bond length of 13.1 Å. However, the hydrogen bonding force of compounds **23b** and **24c** was weaker than the compound **22c**. In particular, the hydrogen bond length between compound **24c** and hinge region residue Met793 were only 2.0 Å and 2.5 Å, respectively, and the length of hydrogen bond formed with Cys797 was only 2.2 Å, which was obviously weaker than the other compounds (**22b**, **23b** and **23g**). The compound **23g** had the strongest binding ability to EGFR<sup>T790M</sup> protein. The length of the hydrogen bond formed with residue Met793 was only 1.7 Å and 2.4 Å, respectively, and the length of the hydrogen bond formed with residue Cys797 was only 1.6 Å. The results of molecular docking study further indicated that the binding modes of compounds **22b** and **23g** to EGFR<sup>T790M</sup> protein were similar to those of the leading compound AZD9291, and the binding abilities were stronger.

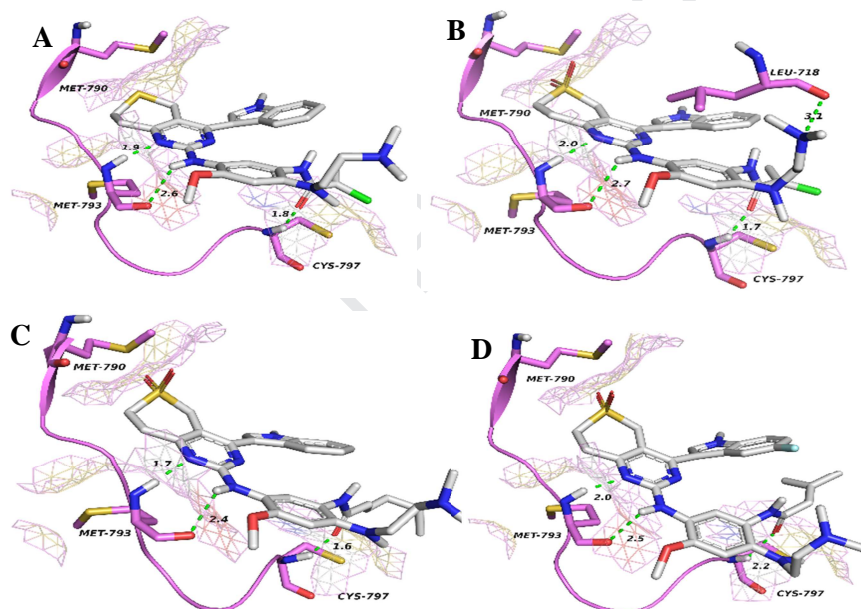


**Figure 4** The docking results of potent compounds bound to EGFR<sup>T790M</sup> protein (PDB code:3IKA). (A: compound **22b**, B: compound **23b**, C: compound **23g**, D: compound **24c**)

#### 2.4.5 Effect on apoptosis

The promising antiproliferative activity of compounds **22b** and **23g** inspired us to further investigate the growth inhibition mechanism of tumor cells. After A549 cells were treated with potent compounds **22b** and **23g** for 48 h, the flow cytometric apoptosis experiments were carried out. The results were shown in **Figure 5**. Compared with the blank group (**Figure 5A**, the total apoptosis rate was 5.25%), the lead compound AZD9291 (**Figure 5B**) significantly induced A549 cells apoptosis at the concentration of 0.462  $\mu$ M, and the total apoptosis rate was 15.24%. The same results were found in compounds **22b** and **23g**. The apoptosis occurred in A549 cells when treated with 0.716  $\mu$ M compounds **22b** and 0.057  $\mu$ M compounds **23g**, respectively. The total apoptosis rates of compounds **22b** and **23g** were 13.55% and

11.79%, respectively. The results of apoptosis indicated that the target compounds **22b** and **23g** significantly induced apoptosis. The inhibition effect was similar to that of the lead compound AZD9291.

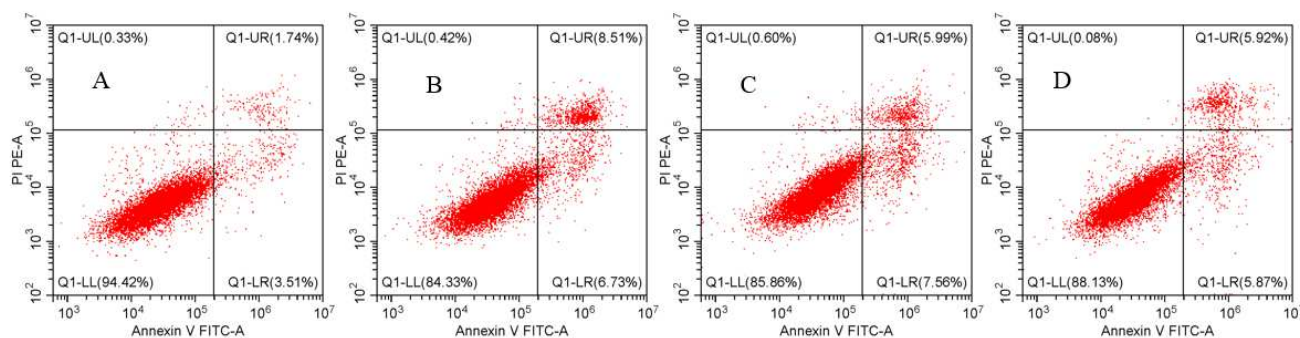


**Figure 5** Cell cycle progression analyses of A549 cells treated with target compounds for 24 h. (A: blank group, B: 0.462  $\mu$ M AZD9291, C: 0.716  $\mu$ M compound **22b**, D: 0.057  $\mu$ M compound **23g**)

#### 2.4.6 Effect on cell cycle progression

To further investigate the mode of cell proliferation inhibition by compound **22b** and **23g**, cell cycle distribution analyses were implemented on A549 cancer cells. The results were presented in **Figure 6**. Except for the blank group, the experimental concentrations of all compounds were the  $IC_{50}$  values for A549 cells (See Table 1 for detailed data). As shown in **Figure 6A**, the G2/M phase population of the blank group was 3.45%. After treatment with AZD9291 (**Figure 6B**), compound **22b** (**Figure 6C**) and compound **23g** (**Figure 6D**), the G2/M phase population of the A549 cancer cells were all increased, with the G2/M phase population of 14.29%, 12.35% and 10.63%, respectively. However, the S phase not found significant changes. The results indicated that compound **22b** and compound **23g** successfully inhibited A549 cells proliferation at a low concentration.

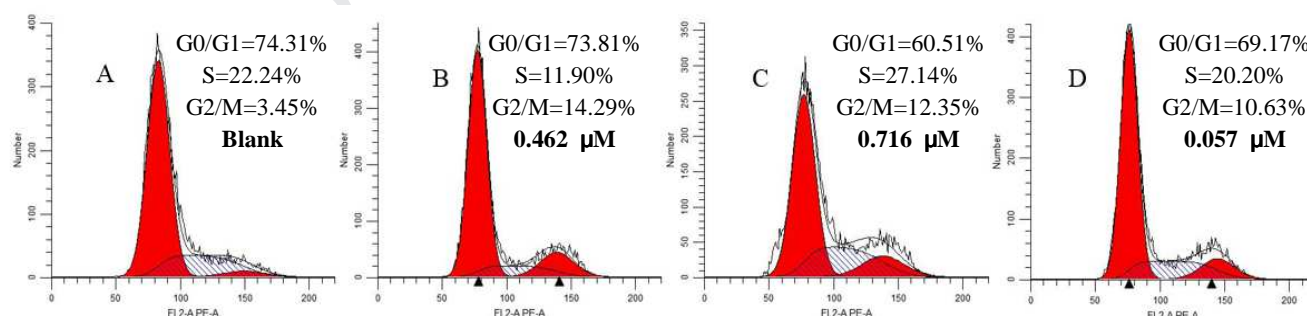


**Figure 6** Apoptosis analyses of A549 cells treated with target compounds for 24 h. (A: blank group, B: 0.462  $\mu$ M AZD9291, C: 0.716  $\mu$ M compound **22b**, D: 0.057  $\mu$ M compound **23g**)

#### 2.4.7 Effect on EGFR signal pathway in Hela cells

To further investigate the effect of the target compound on EGFR signal pathway in Hela cells, the Western Blot assays were carried out. We tested the inhibitory effect of potent compound **23g** on EGFR signal pathway in Hela cells for 24h with the AZD9291 as a positive control. The western blot assays results (**Figure 7**) showed both AZD9291 and

compound **23g** could inhibit the expression of EGFR protein in Hela cells, but the inhibitory effect on phosphorylation of EGFR protein was not obvious. The expression of EGFR protein was significantly inhibited as the concentration of compound **23g** increased. In addition, we also observed that the inhibitory effect of AZD9291 was twice as potent as that of compound **23g**, which was consistent with their kinase activity test results in **Table 2**. The kinase activity test results and western blot assays results further showed that compound **23g** is a potent EGFR inhibitor.

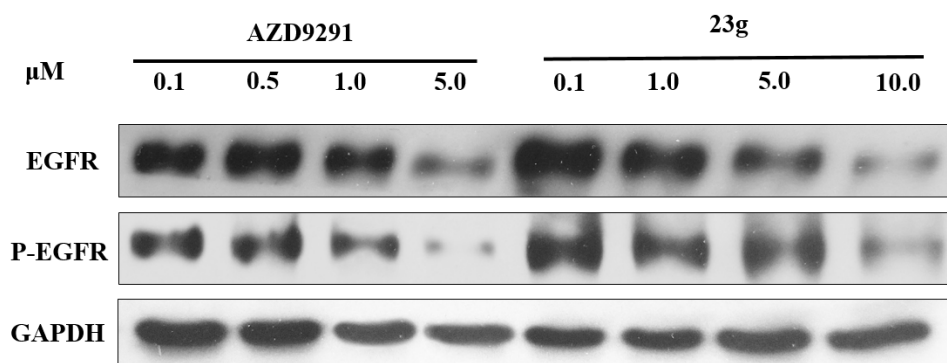


**Figure 7** Effect on EGFR signal pathway in Hela cells for 24h.

## 2.5. 3D-QSAR study

### 2.5.1 3D-QSAR model

All structures of thianopyrimidine derivatives were constructed and aligned onto the common substructure 2-((3-aminophenyl)amino)-7,8-dihydro-5H-thiopyrano[4,3-d]pyrimidine 6,6-dioxide nucleus, with the potent compound **23g** as template (**Figure 8A**). As shown in **Figure 8B**, the structures of all compounds were aligned together. In order to further study the SARs of thianopyrimidine derivatives, the in vitro anti-proliferative activity data of Hela cells were chose to construct the 3D-Quantitative structure activity relationship (3D-QSAR) models. Based on the detailed operation manual reported in the literature<sup>29-31</sup>, the  $\text{IC}_{50}$  values of all compounds against Hela cells were chose and converted to  $\text{pIC}_{50}$  values.

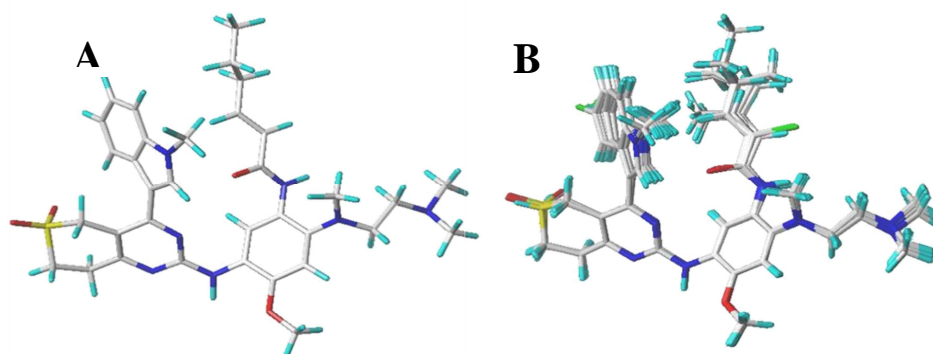


**Figure 8** (A) Structure of the template compound **23g**, (B) 3D-QSAR structure alignment and superposition of all compounds using compound **23g** as the template.

### 2.5.2 CoMFA and CoMSIA analysis

The detailed PLS statistics results of the CoMFA and CoMSIA models were showed in **Table 3**. The experimental and the predicted  $pIC_{50}$  values of the target compounds against Hela cancer cells are listed in **Table 5**. Furthermore, the graphical relationships of CoMFA and CoMSIA models are illustrated in **Figure 9**. The cross-validation correlation coefficient ( $q^2$ ) and correlation coefficient ( $r^2$ ) are two key parameters for evaluating the quality of PLS analysis, which represented the predictive ability and the self-consistence of the model. A  $q^2$  value of more than 0.3 will be considered statistically as the chance of significant correlation being <95%. The detailed PLS data were shown in **Table 3**. The  $q^2$  and  $r^2$  of the CoMFA model were 0.765 and 0.965, respectively, and the  $q^2$  and  $r^2$  of the CoMSIA model were 0.875 and 0.956, respectively. The statistical results revealed that the models of CoMFA and CoMSIA had reliable predictive ability. The optimal numbers of components used to generate CoMFA and CoMSIA models was 8 and 5, respectively. It indicated that the number of compounds used to derive the models were reasonable. The Fisher test results of CoMFA and CoMSIA models were 65.657 and 94.497, respectively. In addition, the estimated standard errors of the CoMFA and CoMSIA models were also reasonably low, reaching to 0.123 and 0.129, respectively. As illustrated in **Table 4**, the contribution of the electrostatic and steric fields of the CoMFA model was 51.6% and 48.4%, respectively. The contribution of the steric, electrostatic, hydrophobic, hydrogen bond donor and acceptor fields of the CoMSIA model were 5.0%, 44.3%, 33.0%, 15.5% and 2.2%, respectively. The PLS data revealed that the CoMFA and CoMSIA models established are reliable and can be used to guide researchers to carry out in-depth and reasonable modification of the target molecules for obtaining better activity.

**Table 4** PLS statistics of CoMFA and CoMSIA 3D-QSAR models.

	$q^2$ <sup>a</sup>	$N$ <sup>b</sup>	$r^2$ <sup>c</sup>	$SE$ <sup>d</sup>	$F$ <sup>e</sup>	Fraction <sup>f</sup>				
						Steric	Electrostatic	Hydrophobic	Donor	Acceptor
CoMFA	0.765	8	0.965	0.123	65.657	0.484	0.516	–	–	–
CoMSIA	0.875	5	0.956	0.129	94.497	0.050	0.443	0.330	0.155	0.022

<sup>a</sup> Cross-validated correlation coefficient;

<sup>b</sup> Optimum number of components obtained from cross-validated PLS analysis and same used in final non-cross-validated analysis;

<sup>c</sup> Non-cross-validated correlation coefficient;

<sup>d</sup> Standard error of estimate;

<sup>e</sup> F-test value. <sup>f</sup> Field contributions.

**Table 5** Experimental and predicted  $pIC_{50}$  values against Hela cell line of compounds for CoMFA and CoMSIA models.

Compd.	$pIC_{50}$ (experimental)	CoMFA		CoMSIA	
		$pIC_{50}$ (predicted)	Residuals	$pIC_{50}$ (predicted)	Residuals
<b>21a</b>	9.138	9.126	0.0166	9.092	0.0462
<b>21b</b>	9.008	9.058	-0.05	9.124	0.116
<b>21c</b>	9.547	9.558	-0.011	9.415	0.1319
<b>21d</b>	9.561	9.594	-0.0329	9.458	0.1032

21e	9.076	9.063	0.0129	9.115	-0.0388
21f	8.877	8.850	0.0275	8.976	-0.0993
21g	9.015	8.975	0.0400	8.944	0.0710
22a	8.887	9.000	-0.1134	9.030	-0.1432
22b	8.998	8.940	0.0581	9.066	-0.0682
22c	8.627	8.661	-0.0342	8.592	0.0353
22d	8.783	8.750	0.0329	8.891	-0.1080
22e	9.097	9.098	-0.0013	9.055	0.0418
22f	9.148	9.059	0.0886	9.006	0.1420
22g	9.186	9.337	-0.1514	9.288	-0.1022
23a	9.939	9.798	0.1409	9.780	0.1592
23b	9.688	9.784	0.096	9.844	0.156
23c	8.345	8.233	0.1121	8.267	0.0782
23d	8.221	8.447	-0.2264	8.322	-0.1007
23e	8.282	8.368	-0.0857	8.353	-0.0706
23f	8.528	8.359	0.1694	8.303	0.2246
23g	9.984	9.981	0.0027	10.049	-0.0646
24a	9.758	9.883	-0.1253	9.820	-0.0616
24b	8.533	8.666	-0.1332	8.540	-0.0073
24c	8.228	8.129	0.0989	8.291	-0.0626
24d	8.607	8.503	0.1042	8.400	0.2070
24e	8.149	8.311	-0.1621	8.395	-0.2461
24f	9.583	9.649	-0.0655	9.741	-0.1576
24g	8.632	8.595	0.0372	8.622	0.0095

The linear correlation results in **Figure 9** revealed that the calculated  $pIC_{50}$  and the experimental  $pIC_{50}$  values of the CoMFA and CoMSIA models had a good linear relationship. In addition, due to structural differences, a small amplitude fluctuations were observed between the calculated  $pIC_{50}$  and the experimental  $pIC_{50}$  values.

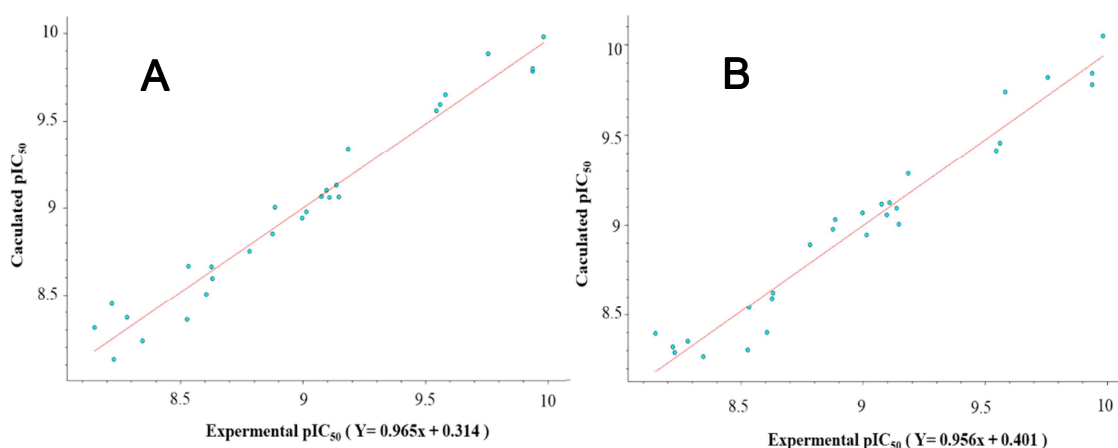


**Figure 9** Calculated  $pIC_{50}$  versus experimental  $pIC_{50}$  values for the target compounds obtained by PLS analysis using CoMFA (**Figure 9A**) and CoMSIA (**Figure 9B**) models.

### 2.5.3 Countour analysis

In order to better reveal the effect of various fields on the target property, by Sybyl 8.1 software, CoMSIA and COMFA contour maps were generated to identify the effects of different fields (the steric field, electrostatic field, hydrophobic field, hydrogen bond donor and acceptor fields) on the activity data of compounds. StDev\*Coeff mapping option was used to convert CoMFA and CoMSIA models into visual results. All contour maps represented 80% level contributions for favored and 20% level contributions for disfavored. As showed in **Figure 10** and **Figure 11**, the template compound **23g** (with the highest pIC<sub>50</sub> value) and the compound **21b** were selected to better reveal the 3D-QSAR information of CoMFA and CoMSIA models. The results can better reveal the relationship between structure and biological activity.

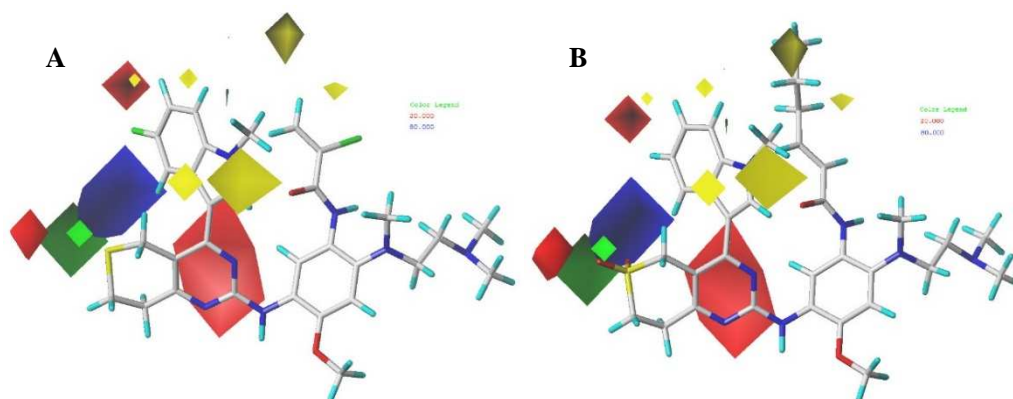


**Figure 10** CoMFA contour maps of target compounds. (A: The CoMFA model of compound **21b**, B: The CoMFA model of compound **23g**. CoMFA steric contours: the green contours indicate the areas that are conducive to steric interaction, the yellow contours indicate the areas that are not conducive to steric interaction. CoMSIA electrostatic contours: the blue contours indicate the regions that are favorable to the positively charged groups, the red contours indicate the regions that are favorable to the negatively charged groups<sup>32</sup>.)

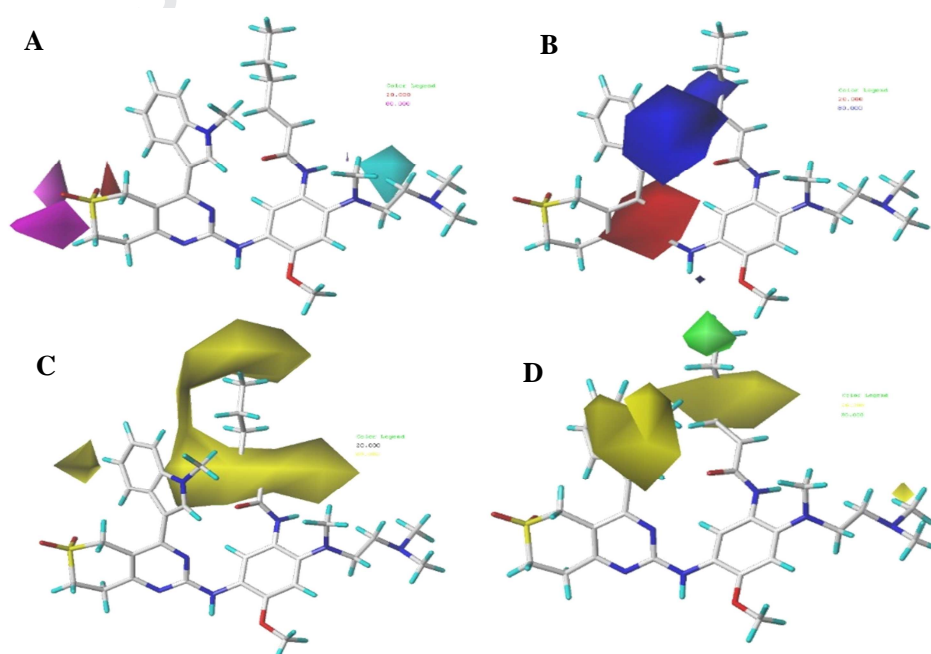


**Figure 11** CoMSIA contour maps of representative compound **23g**. (A: The CoMSIA hydrogen bond donor and acceptor

contours: the cyan and the purple contours represent favorable and unfavorable hydrogen bond donor regions, respectively. The magenta and the red contours represent favorable and unfavorable hydrogen bond acceptor regions, respectively. B: The CoMSIA electrostatic contours: the blue contour indicates electropositive charge and the red contour electronegative charge. C: The CoMSIA hydrophobic contours: the yellow contours represent regions where hydrophobic groups increase activity, while the white contours highlight regions that would favor hydrophilic groups. D: The CoMSIA steric contours: the green contour favors steric or bulky group and the yellow contour denotes disfavored region<sup>32</sup>.)

#### 2.5.4 CoMFA contour analysis.

According to the CoMFA contour maps shown in **Figure 10**, it can be clearly seen that the thiopyran ring was covered with a green contour. The results indicated that increasing the volume of this site (pyrimidine ring) was beneficial to improving the antiproliferative activity of the target compound over Hela cells. Therefore, it is reasonable to introduce the thiopyran structure on the pyrimidine ring. In addition, the result also illustrated the importance of the ring expansion strategy in drug design. The benzene ring structure of the indole ring was covered with a red contour, denoting that the introduction of an electronegative group into indole ring was beneficial to enhance the activity. As shown in **Figure 10**, compound **21a-g** (indole ring with fluorine substitution) had higher anti-proliferative activity of Hela cells than compound **23a-g** (indole ring without fluorine substitution). The results were consistent with the predictions of the CoMFA model. A big red contours appeared around the N-atom of pyrimidine ring and the S-atom of thiopyran ring, respectively, indicating that the thiopyranopyrimidine structure played a key role in maintaining the antiproliferation activity of the target compounds. The appearance of the yellow contours around the acrylamide side chain further explained why the antiproliferative activity of the target compound decreased as the volume of the acrylamide side chain increased. In brief, the CoMFA results are consistent with the antiproliferation activity results of Hela cells (**21c>21e>21g, 23b>23c>23e**) obtained from our experiments.

#### 2.5.5 CoMSIA contour analysis

The steric contours and electrostatic contours of CoMSIA models were similar to the CoMFA models, but there are some differences between CoMSIA and CoMSIA models. In the CoMSIA model, we observed that the blue contours (**Figure 11B**) and the yellow contours (**Figure 11D**) appeared around the N-methylindole ring, indicating that this region would be not suitable for bulkier and more electronegative substituents.

The differences between the CoMSIA model and the CoMFA model were that the CoMSIA model can provide additional hydrogen bond donor and acceptor contours and hydrophobic contours. **Figure 11A** showed the hydrogen bond donor and acceptor contours of the CoMSIA model. A big magenta contour appeared around the S-atom of the

thiopyran ring indicated that the thiopyran ring plays a key role in maintaining the antiproliferative activity of the target compounds. The **Figure 11C** showed that a large number of yellow contours overlapped around the acrylamide side chain. It revealed that the alkylation substitutions of the acrylamide side chain is beneficial to increase the antiproliferative activity against HeLa cells. Similarly, the results of CoMSIA hydrophobic contours are also consistent with the antiproliferation activity results of HeLa cells (**21a>21b, 22a>22b, 23a>23b and 24a>24b**). In addition, the appearance of a small amount of yellow contours around the indole ring indicated that the hydrophobicity of the indole ring was conducive to maintaining the proliferative activity of the compounds against HeLa cells.

### 3. Conclusions

In summary, the structure-based drug design strategy was used to design and synthesize four series of thiopyranopyrimidine AZD9291 derivatives containing acrylamide structure. First, the structure of acrylamide warhead was modified to regulate the reactivity of Michael covalent addition so that the affinity of the medicine to non-target proteins were reduced. Next, the ring expansion principle was applied to expand the volume of the pyrimidine ring. By this way, the affinity of compounds to EGFR protein can be increased. Finally, fluorine element was also introduced into the indole ring to get the optimized compound **23g** with the  $IC_{50}$  values of 0.057  $\mu$ M and 0.104  $\mu$ M against A549 cells and HeLa cells, respectively. The 3D-QSAR results suggested that the introduction of thiopyran skeleton was favorable for increasing the antiproliferative activity of target compounds against HeLa cells. Furthermore, the introduction of bulk alkyl structure on the acrylamide side chain could significantly increase the antiproliferative activity of the target compounds against HeLa cells. The data of CoMFA ( $q^2=0.765$ ,  $r^2=0.965$ ) and CoMSIA ( $q^2=0.875$ ,  $r^2=0.956$ ) models were statistically reliable and could be used in the design of novel and potent double antitumor agents. The further studies on the mechanism of action of these compounds remain in progress and will be published in the future.

### 4. Experimental section

#### 4.1. General methods of chemistry

Unless otherwise required, all solvent and chemicals purchased were analytical grade and used without further purification. Frequently used solvents (DCM, PE and EA, etc.) were resealed to remove water. All chemical reactions were monitored through GF<sub>254</sub> thin-layer chromatography plate and spots were visualized with iodine or light (in 254 nm or 365 nm). The structure of the target compound was confirmed by <sup>1</sup>H NMR and <sup>13</sup>C NMR spectra at room temperature on Bruker 400 MHz spectrometer (Bruker Bioscience, Billerica, MA, USA) with tetramethylsilane (TMS) as an internal standard. Mass spectrometry (MS) was performed on Waters High Resolution Quadrupole Time of Flight Tandem Mass Spectrometry (QTOF). The purity of the compound was determined by Agilent 1260 liquid chromatograph fitted with an

Inertex-C18 column. All target compounds had a purity of  $\geq 95\%$ .

#### 4.1.1. General procedure for the synthesis of **21a-g**

Commercially available starting material 5-fluoroindole **7b** reacted with iodomethane to get **8b**. **10** was obtained by the reaction of self-ester condensation from commercially available **9**. Next, cyclization **10** with urea to obtain **11**. Then, **11** reacted with phosphorus oxychloride to obtain intermediate **12**. Intermediate **12** and **8b** undergone Friedel-Crafts alkylation reaction to obtain intermediate **13b**. **14b** were obtained by the reaction of oxidation reduction from **13b**. The detailed preparation process of the target compounds can be found in our previous research<sup>33,34</sup> or the patent published by AstraZeneca<sup>35</sup>.

##### 4.1.1.1. *N*-(2-((2-(dimethylamino)ethyl)(methyl)amino)-5-((4-(5-fluoro-1-methyl-1H-indol-3-yl)-7,8-dihydro-5H-thiopyrano[4,3-d]pyrimidin-2-yl)amino)-4-methoxyphenyl)acrylamide (**21a**)

Light grayish powder. 48.3% yield, m.p: 268.7-269.2 °C. <sup>1</sup>H NMR (400 MHz, DMSO-*d*<sub>6</sub>)  $\delta$  9.72 (s, 1H, -CO-NH-), 8.60 (s, 1H, -NH-), 8.06–7.93 (m, 2H, indole-H, Ar-H), 7.78 (s, 1H, indole-H), 7.44 (s, 1H, indole-H), 6.98 (s, 2H, indole-H, Ar-H), 6.91 (s, 1H, -CH<sub>2</sub>-CH-), 6.12 (d, *J* = 16.4 Hz, 1H, -CH=CH<sub>2</sub>), 5.61 (d, *J* = 8.2 Hz, 1H, -CH=CH<sub>2</sub>), 3.85 (s, 2H, -S-CH<sub>2</sub>-), 3.82 (s, 3H, -OCH<sub>3</sub>), 3.78 (s, 3H, indole-CH<sub>3</sub>), 3.12 (s, 4H, -S-CH<sub>2</sub>-CH<sub>2</sub>-, -N-CH<sub>3</sub>-CH<sub>2</sub>-), 2.95 (s, 5H, -S-CH<sub>2</sub>-, -N-CH<sub>3</sub>), 2.57 (d, *J* = 11.8 Hz, 8H, N-(CH<sub>3</sub>)<sub>2</sub>, -CH<sub>2</sub>-). TOF MS ES+ (m/z): (M + H)<sup>+</sup>, calcd for C<sub>28</sub>H<sub>32</sub>FN<sub>7</sub>O<sub>2</sub>: 590.2713, found, 590.2735.

##### 4.1.1.2. 2-chloro-*N*-(2-((2-(dimethylamino)ethyl)(methyl)amino)-5-((4-(5-fluoro-1-methyl-1H-indol-3-yl)-7,8-dihydro-5H-thiopyrano[4,3-d]pyrimidin-2-yl)amino)-4-methoxyphenyl)acrylamide (**21b**)

Light grayish powder. 49.7% yield, m.p: 273.2-274.7 °C. <sup>1</sup>H NMR (400 MHz, DMSO-*d*<sub>6</sub>)  $\delta$  9.84 (s, 1H, -CO-NH-), 8.75 (s, 1H, -NH-), 8.07 (s, 1H, indole-H), 8.03 (s, 1H, Ar-H), 7.80 (d, *J* = 10.4 Hz, 1H, indole-H), 7.50–7.46 (m, 1H, indole-H), 7.04 (t, *J* = 9.2, 2.6 Hz, 1H, indole-H), 6.99 (s, 1H, Ar-H), 6.82–6.73 (m, 1H, -C=CH<sub>2</sub>), 6.03 (d, *J* = 15.3 Hz, 1H, -C=CH<sub>2</sub>), 3.90 (s, 2H, -S-CH<sub>2</sub>-), 3.87 (s, 3H, -OCH<sub>3</sub>), 3.80 (s, 3H, indole-CH<sub>3</sub>), 3.00 (dt, *J* = 10.2, 5.2 Hz, 6H, N-(CH<sub>3</sub>)<sub>2</sub>), 2.89 (s, 3H, -N-CH<sub>3</sub>), 2.68 (s, 4H, -S-CH<sub>2</sub>-, -N-CH<sub>3</sub>-CH<sub>2</sub>-), 2.36 (s, 2H, -S-CH<sub>2</sub>-CH<sub>2</sub>-), 2.21–2.15 (m, 2H, -CH<sub>2</sub>-). <sup>13</sup>C NMR (400 MHz, DMSO-*d*<sub>6</sub>)  $\delta$  164.07, 161.95, 160.28, 157.20, 155.46, 147.19, 139.48, 136.09, 135.86, 133.25, 127.59, 127.29, 126.84, 122.84, 115.06, 113.65, 111.94, 111.81, 108.36, 107.97, 97.79, 57.76, 56.15, 52.17, 45.74, 45.71, 38.75, 32.76, 32.33, 30.67, 28.02. TOF MS ES+ (m/z): (M + H)<sup>+</sup>, calcd for C<sub>28</sub>H<sub>32</sub>FN<sub>7</sub>O<sub>2</sub>: 624.2324, found, 624.2313.

##### 4.1.1.3. (*Z*)-*N*-(2-((2-(dimethylamino)ethyl)(methyl)amino)-5-((4-(5-fluoro-1-methyl-1H-indol-3-yl)-7,8-dihydro-5H-thiopyrano[4,3-d]pyrimidin-2-yl)amino)-4-methoxyphenyl)but-2-enamide (**21c**)

Light grayish solid. 50.9% yield, m.p: 271.3-273.8 °C. <sup>1</sup>H NMR (400 MHz, DMSO-*d*<sub>6</sub>) δ 9.86 (s, 1H, -CO-NH-), 8.76 (s, 1H, -NH-), 8.07 (s, 1H, indole-H), 8.03 (d, *J* = 3.2 Hz, 1H, Ar-H), 7.48 (dd, *J* = 8.6, 4.6 Hz, 1H, indole-H), 7.03 (s, 1H, indole-H), 7.00 (d, *J* = 3.4 Hz, 1H, indole-H), 6.72 (dd, *J* = 15.3, 6.3 Hz, 1H, Ar-H), 5.99 (d, *J* = 15.3 Hz, 1H, -CH=C-), 3.90 (s, 2H, -S-CH<sub>2</sub>-), 3.87 (s, 3H, -OCH<sub>3</sub>), 3.81 (s, 3H, indole-CH<sub>3</sub>), 3.05 – 2.97 (m, 5H, -N-CH<sub>3</sub>, -N-CH<sub>3</sub>-CH<sub>2</sub>-), 2.89 (s, 2H, -S-CH<sub>2</sub>-), 2.68 (s, 4H, -CH<sub>2</sub>-, -S-CH<sub>2</sub>-CH<sub>2</sub>-), 2.50 (s, 6H, N-(CH<sub>3</sub>)<sub>2</sub>), 2.28 (s, 6H, C-(CH<sub>3</sub>)<sub>2</sub>). <sup>13</sup>C NMR (400 MHz, DMSO-*d*<sub>6</sub>) δ 166.22, 161.95, 160.28, 157.20, 155.46, 153.52, 147.07, 139.73, 134.92, 133.19, 128.26, 127.25, 126.84, 115.31, 115.00, 113.65, 111.88, 111.80, 109.40, 108.13, 97.85, 57.71, 56.15, 52.20, 45.74, 45.71, 38.72, 32.76, 32.31, 30.67, 28.02, 25.32, 20.70.

4.1.1.4. *N*-(2-((2-(dimethylamino)ethyl)(methyl)amino)-5-((4-(5-fluoro-1-methyl-1*H*-indol-3-yl)-7,8-dihydro-5*H*-thiopyrano[4,3-*d*]pyrimidin-2-yl)amino)-4-methoxyphenyl)-3-methylbut-2-enamide (**21d**)

Light grayish solid. 47.8% yield, m.p: 274.8-276.1 °C. <sup>1</sup>H NMR (400 MHz, DMSO-*d*<sub>6</sub>) δ 9.72 (s, 1H, -CO-NH-), 8.69 (s, 1H, -NH-), 8.06 (s, 1H, indole-H), 8.03 (s, 1H, Ar-H), 7.83–7.78 (m, 1H, indole-H), 7.48 (dd, *J* = 9.0, 4.5 Hz, 1H, indole-H), 7.06–7.00 (m, 1H, indole-H), 6.98 (s, 1H, Ar-H), 6.70 (dt, *J* = 13.9, 7.0 Hz, 1H, -CH-CH<sub>3</sub>), 6.17 (s, 1H, -CO-CH-), 3.90 (s, 2H, -S-CH<sub>2</sub>-), 3.86 (s, 3H, -OCH<sub>3</sub>), 3.81 (s, 3H, indole-CH<sub>3</sub>), 3.03–2.97 (m, 6H, -S-CH<sub>2</sub>-CH<sub>2</sub>-, -N-CH<sub>3</sub>-CH<sub>2</sub>-), 2.65 (s, 5H, -N-CH<sub>3</sub>, -CH<sub>2</sub>-), 2.50 (s, 3H, -CH-CH<sub>3</sub>), 2.36 (s, 6H, N-(CH<sub>3</sub>)<sub>2</sub>). TOF MS ES<sup>+</sup> (*m/z*): (*M* + *H*)<sup>+</sup>, calcd for C<sub>28</sub>H<sub>32</sub>FN<sub>7</sub>O<sub>2</sub>: 618.3026, found, 618.3108.

4.1.1.5. (*Z*)-*N*-(2-((2-(dimethylamino)ethyl)(methyl)amino)-5-((4-(5-fluoro-1-methyl-1*H*-indol-3-yl)-7,8-dihydro-5*H*-thiopyrano[4,3-*d*]pyrimidin-2-yl)amino)-4-methoxyphenyl)pent-2-enamide (**21e**)

Light grayish solid. 47.2% yield, m.p: 273.8-275.2 °C. <sup>1</sup>H NMR (400 MHz, DMSO-*d*<sub>6</sub>) δ 9.76 (s, 1H, -CO-NH-), 8.75 (s, 1H, -NH-), 8.10 (s, 1H, indole-H), 8.07 (s, 1H, Ar-H), 7.84 (d, *J* = 11.2 Hz, 1H, indole-H), 7.51 (dd, *J* = 8.5, 4.8 Hz, 1H, indole-H), 7.07–7.03 (m, 1H, indole-H), 6.95 (d, *J* = 5.1 Hz, 1H, Ar-H), 6.77 (dt, *J* = 13.2, 6.3 Hz, 1H, -CO-CH=CH-), 6.15 (s, 1H, -CO-CH=), 3.92 (s, 2H, -S-CH<sub>2</sub>-), 3.89 (s, 3H, -OCH<sub>3</sub>), 3.82 (s, 3H, indole-CH<sub>3</sub>), 3.09 (dd, *J* = 7.7, 4.2 Hz, 5H, -N-CH<sub>3</sub>, -S-CH<sub>2</sub>-), 2.68 (s, 4H, -CH<sub>2</sub>-, -S-CH<sub>2</sub>-CH<sub>2</sub>-), 2.35 (s, 6H, N-(CH<sub>3</sub>)<sub>2</sub>), 2.14 (q, *J* = 6.3 Hz, 4H, -CH<sub>2</sub>-CH<sub>3</sub>, -N-CH<sub>3</sub>-CH<sub>2</sub>-), 1.01 (t, *J* = 7.3 Hz, 3H, -CH<sub>2</sub>-CH<sub>3</sub>). <sup>13</sup>C NMR (400 MHz, DMSO-*d*<sub>6</sub>) δ 165.14, 161.95, 158.27, 157.20, 155.42, 147.84, 147.07, 139.73, 135.03, 133.35, 128.14, 127.25, 126.91, 120.58, 115.09, 113.65, 112.00, 111.80, 109.40, 108.13, 97.79, 57.85, 56.15, 51.77, 45.74, 45.44, 38.77, 32.73, 32.17, 30.69, 28.09, 22.95, 12.08.

4.1.1.6. (*Z*)-*N*-(2-((2-(dimethylamino)ethyl)(methyl)amino)-5-((4-(5-fluoro-1-methyl-1*H*-indol-3-yl)-7,8-dihydro-5*H*-thiopyrano[4,3-*d*]pyrimidin-2-yl)amino)-4-methoxyphenyl)-4-methylpent-2-enamide (**21f**)

Light grayish solid. 51.8% yield, m.p: 278.4-279.6 °C. <sup>1</sup>H NMR (400 MHz, DMSO-*d*<sub>6</sub>) δ 9.87 (s, 1H, -CO-NH-), 8.76 (s, 1H, -NH-), 8.07 (s, 1H, indole-H), 8.03 (s, 1H, Ar-H), 7.79 (d, *J* = 11.0 Hz, 1H, indole-H), 7.48 (dd, *J* = 8.9, 4.6 Hz, 1H

indole-H), 7.04 (d,  $J = 8.7$  Hz, 1H, indole-H), 6.99 (s, 1H, Ar-H), 6.72 (dd,  $J = 15.1, 6.4$  Hz, 1H, -CO-CH=), 5.99 (d,  $J = 16.1$  Hz, 1H, -CO-CH=CH-), 3.90 (s, 2H, -S-CH<sub>2</sub>-), 3.87 (s, 3H, -OCH<sub>3</sub>), 3.81 (s, 3H, indole-CH<sub>3</sub>), 3.05–2.97 (m, 4H, -N-CH<sub>3</sub>-CH<sub>2</sub>-, -S-CH<sub>2</sub>-), 2.89 (s, 2H, -S-CH<sub>2</sub>-CH<sub>2</sub>-), 2.68 (s, 3H, -N-CH<sub>3</sub>), 2.45 (s, 2H, -CH<sub>2</sub>-), 2.28 (s, 6H, N-(CH<sub>3</sub>)<sub>2</sub>), 2.18 (t,  $J = 7.5$  Hz, 1H, CH-(CH<sub>3</sub>)<sub>2</sub>), 1.05 (d,  $J = 6.8$  Hz, 6H, CH-(CH<sub>3</sub>)<sub>2</sub>). <sup>13</sup>C NMR (400 MHz, DMSO-*d*<sub>6</sub>)  $\delta$  164.50, 161.95, 158.25, 157.20, 155.46, 147.07, 146.71, 139.55, 135.04, 133.25, 128.15, 127.25, 126.84, 121.93, 115.07, 113.65, 112.02, 111.76, 109.36, 108.36, 97.79, 57.79, 56.15, 52.15, 45.74, 45.71, 38.72, 33.04, 32.19, 31.15, 30.38, 27.97, 21.52, 21.18.

4.1.1.7. (Z)-N-(2-((2-(dimethylamino)ethyl)(methyl)amino)-5-((4-(5-fluoro-1-methyl-1H-indol-3-yl)-7,8-dihydro-5H-thiopyrano[4,3-d]pyrimidin-2-yl)amino)-4-methoxyphenyl)hex-2-enamide (**21g**)

Light grayish solid. 50.4% yield, m.p: 279.6–281.2 °C. <sup>1</sup>H NMR (400 MHz, DMSO-*d*<sub>6</sub>)  $\delta$  9.78 (s, 1H, -CO-NH-), 8.72 (s, 1H, -NH-), 8.07 (s, 1H, indole-H), 8.03 (s, 1H, Ar-H), 7.80 (d,  $J = 10.7$  Hz, 1H, indole-H), 7.48 (dd,  $J = 8.9, 4.6$  Hz, 1H, indole-H), 7.07–7.01 (m, 1H, indole-H), 6.99 (d,  $J = 5.5$  Hz, 1H, -CO-CH=CH-), 6.71 (dt,  $J = 14.7, 6.8$  Hz, 1H, -CO-CH=), 6.12 (s, 1H, Ar-H), 3.90 (s, 2H, -S-CH<sub>2</sub>-), 3.87 (s, 3H, -OCH<sub>3</sub>), 3.81 (s, 3H, indole-CH<sub>3</sub>), 3.00 (dd,  $J = 7.8, 4.4$  Hz, 5H, -S-CH<sub>2</sub>-, -N-CH<sub>3</sub>), 2.66 (s, 4H, -S-CH<sub>2</sub>-CH<sub>2</sub>-, -N-CH<sub>3</sub>-CH<sub>2</sub>-), 2.33 (s, 6H, N-(CH<sub>3</sub>)<sub>2</sub>), 2.18 (q,  $J = 6.5$  Hz, 4H, -CH<sub>2</sub>-CH<sub>2</sub>-CH<sub>3</sub>, -CH<sub>2</sub>-), 1.46 (d,  $J = 7.3$  Hz, 2H, -CH<sub>2</sub>-CH<sub>3</sub>), 0.91 (t,  $J = 7.3$  Hz, 3H, -CH<sub>2</sub>-CH<sub>3</sub>). TOF MS ES+ (m/z): (M + H)<sup>+</sup>, calcd for C<sub>28</sub>H<sub>32</sub>FN<sub>7</sub>O<sub>2</sub>: 632.3183, found, 632.3195.

4.1.2. General procedure for the synthesis of **22a-g**

The synthetic methods of compounds **22a-g** are similarly to **21a-g**. The difference is that we need to replace the 5-fluoroindole with indole and the rest of the synthesis conditions are the same.

4.1.2.1. N-(2-((2-(dimethylamino)ethyl)(methyl)amino)-4-methoxy-5-((4-(1-methyl-1H-indol-3-yl)-7,8-dihydro-5H-thiopyrano[4,3-d]pyrimidin-2-yl)amino)phenyl)acrylamide (**22a**)

Light yellow solid. 51.2% yield, m.p: 256.8–258.1 °C. <sup>1</sup>H NMR (400 MHz, DMSO-*d*<sub>6</sub>)  $\delta$  9.90 (s, 1H, -CO-NH-), 9.20 (s, 1H, -NH-), 8.40 (s, 1H, indole-H), 8.34 (s, 1H, indole-H), 8.03 (s, 1H, indole-H), 7.51 (d,  $J = 6.8$  Hz, 1H, Ar-H), 7.23 (t,  $J = 7.0$  Hz, 2H, indole-H), 7.09 (t,  $J = 8.0$  Hz, 1H, Ar-H), 7.00 (s, 1H, -CH=CH<sub>2</sub>), 6.18 (d,  $J = 17.1$  Hz, 1H, -CH=CH<sub>2</sub>), 5.66 (d,  $J = 10.9$  Hz, 1H, -CH=CH<sub>2</sub>), 3.97 (s, 2H, -S-CH<sub>2</sub>-), 3.89 (s, 3H, -OCH<sub>3</sub>), 3.83 (s, 3H, indole-CH<sub>3</sub>), 3.33 (s, 2H, -N-CH<sub>3</sub>-CH<sub>2</sub>-), 3.13 (s, 2H, -S-CH<sub>2</sub>-), 3.00 (s, 2H, -S-CH<sub>2</sub>-CH<sub>2</sub>-), 2.71 (d,  $J = 14.2$  Hz, 8H, -CH<sub>2</sub>-, N-(CH<sub>3</sub>)<sub>2</sub>), 2.63 (s, 3H, -N-CH<sub>3</sub>). <sup>13</sup>C NMR (400 MHz, DMSO-*d*<sub>6</sub>)  $\delta$  164.73, 161.95, 157.20, 154.43, 147.80, 139.70, 136.39, 132.41, 128.24, 127.84, 127.18, 127.16, 126.03, 122.99, 121.92, 120.08, 115.66, 113.62, 110.18, 109.38, 97.81, 57.71, 56.15, 52.20, 45.78, 45.74, 38.72, 32.73, 32.34, 30.63, 28.02.

4.1.2.2. 2-chloro-N-(2-((2-(dimethylamino)ethyl)(methyl)amino)-4-methoxy-5-((4-(1-methyl-1H-indol-3-yl)-7,8-

*dihydro-5H-thiopyrano[4,3-d]pyrimidin-2-yl)amino)phenyl)acrylamide (22b)*

Light yellow solid. 52.4% yield, m.p: 258.6-259.9 °C. <sup>1</sup>H NMR (400 MHz, DMSO-*d*<sub>6</sub>) δ 9.80 (s, 1H, -CO-NH-), 8.67 (s, 1H, -NH-), 8.10–8.05 (m, 2H, indole-H), 7.51 (d, *J* = 8.1 Hz, 1H, indole-H), 7.22 (s, 1H, Ar-H), 7.11 (d, *J* = 9.2 Hz, 2H, indole-H), 7.04 (s, 1H, Ar-H), 6.52 (s, 1H, -C=CH<sub>2</sub>), 6.08 (s, 1H, -C=CH<sub>2</sub>), 3.94 (s, 2H, -S-CH<sub>2</sub>-), 3.90 (s, 3H, -OCH<sub>3</sub>), 3.88 (s, 3H, indole-CH<sub>3</sub>), 3.17 (s, 2H, -N-CH<sub>3</sub>-CH<sub>2</sub>-), 3.07 (s, 2H, -S-CH<sub>2</sub>-), 3.02–3.00 (m, 2H, -S-CH<sub>2</sub>-CH<sub>2</sub>-), 2.77 (s, 6H, N-(CH<sub>3</sub>)<sub>2</sub>), 2.73 (s, 2H, -CH<sub>2</sub>-), 2.63 (s, 3H, -N-CH<sub>3</sub>). <sup>13</sup>C NMR (400 MHz, DMSO-*d*<sub>6</sub>) δ 164.07, 161.95, 157.20, 154.38, 147.90, 139.48, 136.64, 135.86, 132.49, 127.59, 127.29, 126.03, 122.84, 122.42, 121.98, 120.14, 115.66, 113.64, 110.18, 108.51, 97.66, 57.79, 56.15, 52.15, 45.76, 45.72, 38.75, 32.73, 32.31, 30.64, 28.02. TOF MS ES+ (m/z): (M + H)<sup>+</sup>, calcd for C<sub>28</sub>H<sub>32</sub>N<sub>7</sub>O<sub>2</sub>: 606.2418, found, 606.2411.

4.1.2.3. *(Z)-N-(2-((2-(dimethylamino)ethyl)(methyl)amino)-4-methoxy-5-((4-(1-methyl-1H-indol-3-yl)-7,8-dihydro-5H-thiopyrano[4,3-d]pyrimidin-2-yl)amino)phenyl)but-2-enamide (22c)*

Light yellow solid. 47.9% yield, m.p: 257.2-259.3 °C. <sup>1</sup>H NMR (400 MHz, DMSO-*d*<sub>6</sub>) δ 10.22 (s, 1H, -CO-NH-), 9.11 (s, 1H, -NH-), 8.11 (d, *J* = 8.0 Hz, 1H, indole-H), 7.85 (dd, *J* = 8.2, 4.3 Hz, 1H, indole-H), 7.68 (d, *J* = 8.4 Hz, 1H, Ar-H), 7.25 (t, *J* = 7.7 Hz, 1H, indole-H), 7.18 (s, 1H, indole-H), 6.88 (s, 1H, indole-H), 6.47 (s, 1H, Ar-H), 6.09 (s, 1H, -CO-CH), 3.87 (s, 3H, -OCH<sub>3</sub>), 3.72 (s, 3H, indole-CH<sub>3</sub>), 3.68 (s, 2H, -S-CH<sub>2</sub>-), 3.36 (s, 4H, -N-CH<sub>3</sub>-CH<sub>2</sub>-, -S-CH<sub>2</sub>-), 3.20 (d, *J* = 5.9 Hz, 2H, -S-CH<sub>2</sub>-CH<sub>2</sub>-), 2.96 (s, 3H, -N-CH<sub>3</sub>), 2.72 (s, 2H, -CH<sub>2</sub>-), 2.65 (s, 6H, N-(CH<sub>3</sub>)<sub>2</sub>), 2.34 (s, 3H, -CH-(CH<sub>3</sub>)<sub>2</sub>), 2.21 (s, 3H, -CH-(CH<sub>3</sub>)<sub>2</sub>). <sup>13</sup>C NMR (400 MHz, DMSO-*d*<sub>6</sub>) δ 166.15, 161.95, 157.20, 154.43, 153.52, 147.80, 139.74, 136.52, 132.51, 128.56, 127.17, 126.03, 122.49, 121.89, 120.03, 115.71, 115.39, 113.64, 110.13, 109.38, 97.79, 57.79, 56.15, 52.15, 45.74, 45.71, 38.75, 32.73, 32.34, 30.63, 28.02, 25.32, 20.76.

4.1.2.4. *N-(2-((2-(dimethylamino)ethyl)(methyl)amino)-4-methoxy-5-((4-(1-methyl-1H-indol-3-yl)-7,8-dihydro-5H-thiopyrano[4,3-d]pyrimidin-2-yl)amino)phenyl)-3-methylbut-2-enamide (22d)*

Light yellow solid. 47.3% yield, m.p: 256.7-258.2 °C. <sup>1</sup>H NMR (400 MHz, DMSO-*d*<sub>6</sub>) δ 10.23 (s, 1H, -CO-NH-), 9.85 (s, 1H, -NH-), 8.67 (s, 1H, indole-H), 8.08 (d, *J* = 8.0 Hz, 1H, indole-H), 8.03 (s, 1H, Ar-H), 7.62 (dd, *J* = 8.0, 4.7 Hz, 1H, indole-H), 7.51 (d, *J* = 8.1 Hz, 1H, indole-H), 7.22 (t, *J* = 7.7 Hz, 1H, indole-H), 7.13 (t, *J* = 7.7 Hz, 1H, =CH-CH<sub>3</sub>), 6.92 (s, 1H, Ar-H), 6.78 (d, *J* = 5.9 Hz, 1H, -CO-CH=), 3.95 (s, 2H, -S-CH<sub>2</sub>-), 3.90 (s, 3H, -OCH<sub>3</sub>), 3.88 (s, 3H, indole-CH<sub>3</sub>), 3.35 (s, 4H, -N-CH<sub>3</sub>-CH<sub>2</sub>-, -S-CH<sub>2</sub>-), 3.13 (d, *J* = 6.8 Hz, 3H, -N-CH<sub>3</sub>), 3.02 (d, *J* = 6.3 Hz, 2H, -S-CH<sub>2</sub>-CH<sub>2</sub>-), 2.75 (s, 6H, N-(CH<sub>3</sub>)<sub>2</sub>), 2.72 (s, 2H, -CH<sub>2</sub>-), 2.66 (s, 3H, -CH-CH<sub>3</sub>). TOF MS ES+ (m/z): (M + H)<sup>+</sup>, calcd for C<sub>28</sub>H<sub>32</sub>N<sub>7</sub>O<sub>2</sub>: 600.3121, found, 600.3231.

4.1.2.5. *(Z)-N-(2-((2-(dimethylamino)ethyl)(methyl)amino)-4-methoxy-5-((4-(1-methyl-1H-indol-3-yl)-7,8-dihydro-5H-thiopyrano[4,3-d]pyrimidin-2-yl)amino)phenyl)pent-2-enamide (22e)*

Light yellow solid. 49.1% yield, m.p: 261.3-1263.4 °C.  $^1\text{H}$  NMR (400 MHz, DMSO- $d_6$ )  $\delta$  10.55 (s, 1H, -CO-NH-), 9.59 (s, 1H, -NH-), 8.64 (s, 1H, indole-H), 8.06 (d,  $J$  = 8.0 Hz, 1H, indole-H), 8.02 (s, 1H, Ar-H), 7.54 (dd,  $J$  = 8.0, 4.7 Hz, 1H, indole-H), 7.48 (d,  $J$  = 8.3 Hz, 1H, indole-H), 7.19 (t,  $J$  = 7.6 Hz, 1H, indole-H), 7.09 (t,  $J$  = 7.5 Hz, 1H, =CH-CH<sub>2</sub>-CH<sub>3</sub>), 6.92 (s, 1H, Ar-H), 6.78 (d,  $J$  = 5.4 Hz, 1H, -CO-CH=), 3.91 (s, 2H, -S-CH<sub>2</sub>-), 3.87 (s, 3H, -OCH<sub>3</sub>), 3.85 (s, 3H, indole-CH<sub>3</sub>), 3.25 (s, 2H, -N-CH<sub>3</sub>-CH<sub>2</sub>-), 3.01 (dd,  $J$  = 12.8, 5.3 Hz, 4H, -S-CH<sub>2</sub>-, -S-CH<sub>2</sub>-CH<sub>2</sub>-), 2.74 (s, 2H, -CH<sub>2</sub>-), 2.71 (s, 6H, N-(CH<sub>3</sub>)<sub>2</sub>), 2.57 (s, 3H, -N-CH<sub>3</sub>), 2.20 (p,  $J$  = 6.7 Hz, 2H, -CH<sub>2</sub>-CH<sub>3</sub>), 1.05 (t,  $J$  = 7.4 Hz, 3H, -CH<sub>2</sub>-CH<sub>3</sub>).  $^{13}\text{C}$  NMR (400 MHz, DMSO- $d_6$ )  $\delta$  165.06, 161.95, 157.20, 154.38, 147.80, 147.72, 139.73, 136.47, 132.45, 128.40, 127.17, 126.09, 122.36, 121.89, 120.54, 119.60, 115.82, 113.64, 110.13, 109.38, 97.64, 57.79, 56.15, 52.20, 46.29, 45.37, 38.72, 32.73, 32.35, 30.63, 27.97, 22.96, 12.22. TOF MS ES+ (m/z): (M + H)<sup>+</sup>, calcd for C<sub>28</sub>H<sub>32</sub>FN<sub>7</sub>O<sub>2</sub>: 600.3121, found, 600.3120.

4.1.2.6 (Z)-N-(2-((2-(dimethylamino)ethyl)(methylamino)-4-methoxy-5-((4-(1-methyl-1H-indol-3-yl)-7,8-dihydro-5H-thiopyrano[4,3-d]pyrimidin-2-yl)amino)phenyl)-4-methylpent-2-enamide (22f)

Light yellow solid. 42.9% yield, m.p: 260.8-262.4 °C.  $^1\text{H}$  NMR (400 MHz, DMSO- $d_6$ )  $\delta$  10.32 (s, 1H, -CO-NH-), 9.21 (s, 1H, -NH-), 8.08 (d,  $J$  = 8.0 Hz, 1H, indole-H), 7.81 (dd,  $J$  = 8.0, 4.7 Hz, 1H, indole-H), 7.61 (d,  $J$  = 8.3 Hz, 1H, Ar-H), 7.21 (t,  $J$  = 7.6 Hz, 1H, indole-H), 7.13 (s, 1H, indole-H), 6.92 (s, 1H, indole-H), 6.51 (s, 1H, Ar-H), 6.21 (d,  $J$  = 5.4 Hz, 2H, -CO-CH=CH-), 3.97 (s, 3H, -OCH<sub>3</sub>), 3.80 (s, 3H, indole-CH<sub>3</sub>), 3.78 (s, 2H, -S-CH<sub>2</sub>-), 3.40 (s, 4H, -N-CH<sub>3</sub>-CH<sub>2</sub>-, -S-CH<sub>2</sub>-), 3.22 (d,  $J$  = 5.9 Hz, 2H, -S-CH<sub>2</sub>-CH<sub>2</sub>-), 3.02 (s, 3H, -N-CH<sub>3</sub>), 2.75 (s, 6H, N-(CH<sub>3</sub>)<sub>2</sub>), 2.72 (s, 2H, -CH<sub>2</sub>-), 2.68 (s, 1H, -CH-(CH<sub>3</sub>)<sub>2</sub>), 1.03 (s, 3H, -CH-(CH<sub>3</sub>)<sub>2</sub>), 1.01 (s, 3H, -CH-(CH<sub>3</sub>)<sub>2</sub>).  $^{13}\text{C}$  NMR (400 MHz, DMSO- $d_6$ )  $\delta$  164.50, 161.95, 157.20, 154.38, 147.80, 146.75, 139.54, 136.37, 132.51, 128.14, 127.25, 126.09, 122.81, 121.93, 121.34, 119.86, 115.72, 113.64, 110.13, 109.40, 97.85, 57.79, 56.15, 52.20, 45.92, 45.35, 38.61, 32.73, 32.01, 31.10, 30.48, 28.02, 21.52, 21.06.

4.1.2.7 (Z)-N-(2-((2-(dimethylamino)ethyl)(methylamino)-4-methoxy-5-((4-(1-methyl-1H-indol-3-yl)-7,8-dihydro-5H-thiopyrano[4,3-d]pyrimidin-2-yl)amino)phenyl)hex-2-enamide (22g)

Light yellow solid. 43.6% yield, m.p: 263.4-265.1 °C.  $^1\text{H}$  NMR (400 MHz, DMSO- $d_6$ )  $\delta$  9.84 (s, 1H, -CO-NH-), 8.89 (s, 1H, -NH-), 8.04 (d,  $J$  = 8.1 Hz, 1H, indole-H), 7.99 (s, 1H, indole-H), 7.84 (s, 1H, Ar-H), 7.47 (d,  $J$  = 8.2 Hz, 1H, indole-H), 7.18 (t,  $J$  = 7.6 Hz, 1H, indole-H), 7.04 (t,  $J$  = 7.7 Hz, 1H, indole-H), 6.98 (s, 1H, Ar-H), 6.76 (dt,  $J$  = 14.7, 6.9 Hz, 1H, -CO-CH=), 6.07 (d,  $J$  = 15.2 Hz, 1H, -CO-CH=CH-), 3.90 (s, 2H, -S-CH<sub>2</sub>-), 3.87 (s, 3H, -OCH<sub>3</sub>), 3.82 (s, 3H, indole-CH<sub>3</sub>), 3.06-2.97 (m, 4H, -N-CH<sub>3</sub>-CH<sub>2</sub>-, -S-CH<sub>2</sub>-), 2.90 (s, 2H, -S-CH<sub>2</sub>-CH<sub>2</sub>-), 2.67 (s, 3H, -N-CH<sub>3</sub>), 2.42 (s, 2H, -CH<sub>2</sub>-), 2.32-2.13 (m, 8H, N-(CH<sub>3</sub>)<sub>2</sub>, -CH<sub>2</sub>-CH<sub>2</sub>-CH<sup>3</sup>), 1.47 (dt,  $J$  = 14.6, 7.3 Hz, 2H, -CH<sub>2</sub>-CH<sub>2</sub>-CH<sub>3</sub>), 0.92 (t,  $J$  = 7.3 Hz, 3H, -CH<sub>2</sub>-CH<sub>2</sub>-CH<sub>3</sub>). TOF MS ES+ (m/z): (M + H)<sup>+</sup>, calcd for C<sub>28</sub>H<sub>32</sub>FN<sub>7</sub>O<sub>2</sub>: 614.3277, found, 614.3276.

4.1.3. General procedure for the synthesis of **23a-g**

The synthetic methods of compounds **23a-g** are similarly to **22a-g**. The difference is that we need to replace the intermediate **13b** with intermediate **14a** and the rest of the synthesis conditions are the same.

4.1.3.1. *N*-(2-((2-(dimethylamino)ethyl)(methyl)amino)-4-methoxy-5-((4-(1-methyl-1H-indol-3-yl)-6,6-dioxido-7,8-dihydro-5H-thiopyrano[4,3-d]pyrimidin-2-yl)amino)phenyl)acrylamide (**23a**)

Light yellow solid. 38.9% yield, m.p: 238.7-240.2 °C. <sup>1</sup>H NMR (400 MHz, DMSO-*d*<sub>6</sub>) δ 9.93 (s, 1H, -CO-NH-), 8.70 (s, 1H, -NH-), 8.19 (s, 1H, indole-H), 8.05 (d, *J* = 8.2 Hz, 1H, indole-H), 7.96 (s, 1H, Ar-H), 7.49 (d, *J* = 8.3 Hz, 1H, indole-H), 7.20 (t, *J* = 7.6 Hz, 1H, indole-H), 7.06 (t, *J* = 7.6 Hz, 1H, indole-H), 6.99 (s, 1H, Ar-H), 6.66 (s, 1H, -CH=CH<sub>2</sub>), 6.22 (d, *J* = 16.8 Hz, 1H, -CH=CH<sub>2</sub>), 5.72 (d, *J* = 10.4 Hz, 1H, -CH=CH<sub>2</sub>), 4.48 (s, 2H, -SO<sub>2</sub>-CH<sub>2</sub>-), 3.87 (s, 3H, -OCH<sub>3</sub>), 3.83 (s, 3H, indole-CH<sub>3</sub>), 3.58 (t, *J* = 7.0 Hz, 2H, -N-CH<sub>3</sub>-CH<sub>2</sub>-), 3.29 (t, *J* = 7.6 Hz, 4H, -SO<sub>2</sub>-CH<sub>2</sub>-CH<sub>2</sub>-), 3.06 (d, *J* = 13.8 Hz, 2H, -CH<sub>2</sub>-), 2.65 (s, 3H, -N-CH<sub>3</sub>), 2.42 (s, 6H, N-(CH<sub>3</sub>)<sub>2</sub>). TOF MS ES+ (m/z): (M + H)<sup>+</sup>, calcd for C<sub>28</sub>H<sub>32</sub>FN<sub>7</sub>O<sub>2</sub>: 604.2706, found, 604.2710.

4.1.3.2. 2-chloro-*N*-(2-((2-(dimethylamino)ethyl)(methyl)amino)-4-methoxy-5-((4-(1-methyl-1H-indol-3-yl)-6,6-dioxido-7,8-dihydro-5H-thiopyrano[4,3-d]pyrimidin-2-yl)amino)phenyl)acrylamide (**23b**)

Light yellow solid. 39.7% yield, m.p: 239.8-241.1 °C. <sup>1</sup>H NMR (400 MHz, DMSO-*d*<sub>6</sub>) δ 9.87 (s, 1H, -CO-NH-), 8.69 (s, 1H, -NH-), 8.14 (s, 1H, indole-H), 8.07 (d, *J* = 8.1 Hz, 1H, indole-H), 7.96 (s, 1H, Ar-H), 7.50 (d, *J* = 8.1 Hz, 1H, indole-H), 7.22 (t, *J* = 7.5 Hz, 1H, indole-H), 7.11 (t, *J* = 7.5 Hz, 1H, indole-H), 7.06 (s, 1H, Ar-H), 6.53 (s, 1H, -C=CH<sub>2</sub>), 6.07 (s, 1H, -C=CH<sub>2</sub>), 4.50 (s, 2H, -SO<sub>2</sub>-CH<sub>2</sub>-), 3.89 (d, *J* = 2.7 Hz, 6H, -OCH<sub>3</sub>, indole-CH<sub>3</sub>), 3.60 (t, *J* = 6.8 Hz, 2H, -N-CH<sub>3</sub>-CH<sub>2</sub>-), 3.32 (d, *J* = 6.3 Hz, 4H, -SO<sub>2</sub>-CH<sub>2</sub>-CH<sub>2</sub>-), 3.00 (s, 3H, -N-CH<sub>3</sub>), 2.63 (s, 6H, N-(CH<sub>3</sub>)<sub>2</sub>), 2.53–2.50 (m, 2H, -CH<sub>2</sub>-). <sup>13</sup>C NMR (400 MHz, DMSO-*d*<sub>6</sub>) δ 164.43, 159.93, 157.92, 155.05, 147.19, 139.48, 136.60, 135.53, 132.51, 127.59, 127.37, 126.03, 122.84, 122.53, 121.76, 120.11, 116.24, 110.13, 108.36, 104.97, 97.79, 57.79, 56.15, 53.42, 52.20, 48.79, 45.74, 45.57, 38.75, 32.70, 29.64. TOF MS ES+ (m/z): (M + H)<sup>+</sup>, calcd for C<sub>28</sub>H<sub>32</sub>FN<sub>7</sub>O<sub>2</sub>: 638.2316, found, 638.2325.

4.1.3.3. (*Z*)-*N*-(2-((2-(dimethylamino)ethyl)(methyl)amino)-4-methoxy-5-((4-(1-methyl-1H-indol-3-yl)-6,6-dioxido-7,8-dihydro-5H-thiopyrano[4,3-d]pyrimidin-2-yl)amino)phenyl)but-2-enamide (**23c**)

Light yellow solid. 36.9% yield, m.p: 234.5-236.9 °C. <sup>1</sup>H NMR (400 MHz, DMSO-*d*<sub>6</sub>) δ 9.69 (s, 1H, -CO-NH-), 8.59 (s, 1H, -NH-), 8.16 (s, 1H, indole-H), 8.11 (d, *J* = 8.0 Hz, 1H, indole-H), 7.93 (s, 1H, Ar-H), 7.51 (d, *J* = 8.3 Hz, 1H, indole-H), 7.19 (t, *J* = 7.7 Hz, 1H, indole-H), 7.07 (t, *J* = 7.5 Hz, 1H, indole-H), 6.97 (s, 1H, Ar-H), 6.78 (dt, *J* = 14.6, 6.7 Hz, 1H, -CO-CH=), 4.51 (s, 2H, -SO<sub>2</sub>-CH<sub>2</sub>-), 3.86 (s, 3H, -OCH<sub>3</sub>), 3.88 (s, 3H, indole-CH<sub>3</sub>), 3.73 (t, *J* = 6.7 Hz, 3H, -N-CH<sub>3</sub>), 3.30 (t, *J* = 7.6 Hz, 2H, -N-CH<sub>3</sub>-CH<sub>2</sub>-), 3.22–3.02 (m, 4H, -SO<sub>2</sub>-CH<sub>2</sub>-CH<sub>2</sub>-), 2.72 (s, 6H, N-(CH<sub>3</sub>)<sub>2</sub>), 2.64 (d, *J* =

13.8 Hz, 2H, -CH<sub>2</sub>-), 2.54 (s, 3H, =C(CH<sub>3</sub>)<sub>2</sub>), 2.31 (s, 3H, =C(CH<sub>3</sub>)<sub>2</sub>). <sup>13</sup>C NMR (400 MHz, DMSO-*d*<sub>6</sub>) δ 166.22, 159.93, 157.92, 155.05, 153.52, 147.07, 139.57, 136.55, 132.51, 128.21, 127.25, 126.03, 122.71, 122.05, 120.08, 116.27, 115.31, 110.05, 109.36, 104.97, 97.85, 57.74, 56.15, 53.42, 52.20, 48.79, 45.74, 45.71, 38.72, 32.73, 29.64, 25.38, 20.76.

4.1.3.4. *N*-(2-((2-(dimethylamino)ethyl)(methyl)amino)-4-methoxy-5-((4-(1-methyl-1H-indol-3-yl)-6,6-dioxido-7,8-dihydro-5H-thiopyrano[4,3-*d*]pyrimidin-2-yl)amino)phenyl)-3-methylbut-2-enamide (**23d**)

Light yellow solid. 40.2% yield, m.p: 235.9-237.2 °C. <sup>1</sup>H NMR (400 MHz, DMSO-*d*<sub>6</sub>) δ 9.63 (s, 1H, -CO-NH-), 8.58 (s, 1H, -NH-), 8.17 (s, 1H, indole-H), 8.03 (d, *J* = 8.0 Hz, 1H, indole-H), 7.93 (s, 1H, Ar-H), 7.47 (d, *J* = 8.3 Hz, 1H, indole-H), 7.18 (t, *J* = 7.7 Hz, 1H, indole-H), 7.05 (t, *J* = 7.5 Hz, 1H, indole-H), 6.93 (s, 1H, Ar-H), 6.74 (dt, *J* = 14.6, 6.7 Hz, 2H, -CO-CH=CH-), 4.46 (s, 2H, -SO<sub>2</sub>-CH<sub>2</sub>-), 3.86 (s, 3H, -OCH<sub>3</sub>), 3.81 (s, 3H, indole-CH<sub>3</sub>), 3.57 (t, *J* = 6.7 Hz, 2H, -N-CH<sub>3</sub>-CH<sub>2</sub>-), 3.28 (d, *J* = 6.5 Hz, 4H, -SO<sub>2</sub>-CH<sub>2</sub>-CH<sub>2</sub>-), 3.22–3.02 (m, 3H, -N-CH<sub>3</sub>), 2.59 (s, 8H, N-(CH<sub>3</sub>)<sub>2</sub>, -CH<sub>2</sub>-), 1.84 (d, *J* = 6.0 Hz, 3H, =CH-CH<sub>3</sub>). TOF MS ES+ (m/z): (M + H)<sup>+</sup>, calcd for C<sub>28</sub>H<sub>32</sub>FN<sub>7</sub>O<sub>2</sub>: 632.3019, found, 632.3026.

4.1.3.5. (*Z*)-*N*-(2-((2-(dimethylamino)ethyl)(methyl)amino)-4-methoxy-5-((4-(1-methyl-1H-indol-3-yl)-6,6-dioxido-7,8-dihydro-5H-thiopyrano[4,3-*d*]pyrimidin-2-yl)amino)phenyl)pent-2-enamide (**23e**)

Light yellow solid. 33.5% yield, m.p: 237.6-239.2 °C. <sup>1</sup>H NMR (400 MHz, DMSO-*d*<sub>6</sub>) δ 9.56 (s, 1H, -CO-NH-), 8.53 (s, 1H, -NH-), 8.16 (s, 1H, indole-H), 8.06 (d, *J* = 7.8 Hz, 1H, indole-H), 7.95 (s, 1H, Ar-H), 7.50 (d, *J* = 7.8 Hz, 1H, indole-H), 7.23–7.17 (m, 1H, indole-H), 7.12–7.05 (m, 1H, indole-H), 6.94 (s, 1H, Ar-H), 6.87–6.75 (m, 1H, -CO-CH=), 6.67 (s, 1H, -CO-CH=CH-), 4.49 (s, 2H, -SO<sub>2</sub>-CH<sub>2</sub>-), 3.88 (s, 3H, -OCH<sub>3</sub>), 3.85 (s, 3H, indole-CH<sub>3</sub>), 3.62–3.55 (m, 2H, -N-CH<sub>3</sub>-CH<sub>2</sub>-), 3.31–3.23 (m, 4H, -SO<sub>2</sub>-CH<sub>2</sub>-CH<sub>2</sub>-), 2.71 (s, 6H, N-(CH<sub>3</sub>)<sub>2</sub>), 2.58 (s, 3H, -N-CH<sub>3</sub>), 2.26–2.14 (m, 2H, -CH<sub>2</sub>-), 1.30 (s, 2H, -CH<sub>2</sub>-CH<sub>3</sub>), 1.06 (t, *J* = 7.1 Hz, 3H, -CH<sub>2</sub>-CH<sub>3</sub>). <sup>13</sup>C NMR (400 MHz, DMSO-*d*<sub>6</sub>) δ 165.14, 159.93, 157.92, 155.00, 147.84, 147.07, 139.57, 136.49, 132.51, 128.14, 127.25, 126.03, 122.71, 122.05, 120.58, 120.03, 116.27, 110.13, 109.36, 104.97, 97.85, 57.79, 56.15, 53.42, 52.20, 48.79, 45.74, 45.31, 38.75, 32.70, 29.64, 23.08, 12.29.

4.1.3.6. (*Z*)-*N*-(2-((2-(dimethylamino)ethyl)(methyl)amino)-4-methoxy-5-((4-(1-methyl-1H-indol-3-yl)-6,6-dioxido-7,8-dihydro-5H-thiopyrano[4,3-*d*]pyrimidin-2-yl)amino)phenyl)-4-methylpent-2-enamide (**23f**)

Light yellow solid. 32.4% yield, m.p: 241.5-243.7 °C. <sup>1</sup>H NMR (400 MHz, DMSO-*d*<sub>6</sub>) δ 10.08 (s, 1H, -CO-NH-), 9.31 (s, 1H, -NH-), 8.37 (d, *J* = 8.9 Hz, 1H, indole-H), 7.71 (d, *J* = 10.9 Hz, 1H, indole-H), 7.55 (dd, *J* = 8.2, 4.7 Hz, 1H, indole-H), 7.44–7.32 (m, 1H, indole-H), 7.08 (s, 1H, Ar-H), 6.95 (s, 1H, indole-H), 6.53 (s, 1H, Ar-H), 6.39–6.20 (dd, *J* = 15.2, 6.2 Hz, 2H, -CO-CH=CH-), 4.49 (s, 2H, -SO<sub>2</sub>-CH<sub>2</sub>-), 3.88 (s, 3H, -OCH<sub>3</sub>), 3.82 (s, 3H, indole-CH<sub>3</sub>), 3.60 (t, *J* = 6.6 Hz, 3H, -N-CH<sub>3</sub>), 3.31 (d, *J* = 5.3 Hz, 6H, -SO<sub>2</sub>-CH<sub>2</sub>-CH<sub>2</sub>-, -N-CH<sub>3</sub>-CH<sub>2</sub>-), 2.72 (s, 6H, N-(CH<sub>3</sub>)<sub>2</sub>), 2.61 (s, 3H, -CH<sub>2</sub>-, -CH-(CH<sub>3</sub>)<sub>2</sub>), 1.01 (d, *J* = 6.3 Hz, 6H, -CH-(CH<sub>3</sub>)<sub>2</sub>). <sup>13</sup>C NMR (400 MHz, DMSO-*d*<sub>6</sub>) δ 164.97, 161.93, 158.92, 154.97, 147.07, 146.74, 139.57, 136.60, 132.51, 128.09, 127.25, 126.09, 122.73, 122.04, 121.87, 120.08, 116.48, 110.13, 109.36,

104.97, 97.80, 57.79, 56.15, 53.39, 52.20, 48.79, 45.74, 45.48, 38.72, 32.73, 31.12, 29.61, 21.54, 21.43.

4.1.3.7. (Z)-N-(2-((2-(dimethylamino)ethyl)(methyl)amino)-4-methoxy-5-((4-(1-methyl-1H-indol-3-yl)-6,6-dioxido-7,8-dihydro-5H-thiopyrano[4,3-d]pyrimidin-2-yl)amino)phenyl)hex-2-enamide (**23g**)

Light yellow solid. 34.5% yield, m.p: 243.2-245.7 °C. <sup>1</sup>H NMR (400 MHz, DMSO-*d*<sub>6</sub>) δ 9.62 (s, 1H, -CO-NH-), 8.58 (s, 1H, -NH-), 8.16 (s, 1H, indole-H), 8.05 (d, *J* = 8.0 Hz, 1H, indole-H), 7.95 (s, 1H, Ar-H), 7.48 (d, *J* = 8.0 Hz, 1H, indole-H), 7.19 (t, *J* = 7.5 Hz, 1H, indole-H), 7.08 (t, *J* = 7.5 Hz, 1H, indole-H), 6.93 (s, 1H, Ar-H), 6.75 (s, 2H, -CO-CH=CH-), 4.48 (s, 2H, -SO<sub>2</sub>-CH<sub>2</sub>-), 3.87 (s, 3H, -OCH<sub>3</sub>), 3.83 (s, 3H, indole-CH<sub>3</sub>), 3.58 (t, *J* = 6.6 Hz, 2H, -N-CH<sub>3</sub>-CH<sub>2</sub>-), 3.28 (t, *J* = 6.5 Hz, 2H, -SO<sub>2</sub>-CH<sub>2</sub>-), 3.26–3.16 (m, 2H, -SO<sub>2</sub>-CH<sub>2</sub>-CH<sub>2</sub>-), 2.65 (s, 6H, N-(CH<sub>3</sub>)<sub>2</sub>), 2.58 (s, 3H, -N-CH<sub>3</sub>), 2.16 (q, *J* = 6.5 Hz, 2H, -CH<sub>2</sub>-), 1.47 (h, *J* = 6.3, 5.9 Hz, 2H, -CH<sub>2</sub>-CH<sub>2</sub>-CH<sub>3</sub>), 1.24 (d, *J* = 8.9 Hz, 2H, -CH<sub>2</sub>-CH<sub>2</sub>-CH<sub>3</sub>), 0.92 (t, *J* = 7.2 Hz, 3H, -CH<sub>2</sub>-CH<sub>2</sub>-CH<sub>3</sub>). <sup>13</sup>C NMR (400 MHz, DMSO-*d*<sub>6</sub>) δ 163.87, 162.00, 161.50, 158.83, 147.87, 143.34, 139.51, 136.70, 133.42, 126.45, 126.07, 125.43, 124.43, 122.11, 121.99, 120.64, 118.14, 110.55, 109.96, 108.97, 104.54, 56.02, 50.54, 46.69, 42.82, 42.44, 33.39, 32.90, 32.14, 31.13, 29.83, 28.95, 21.14, 13.61. TOF MS ES<sup>+</sup> (m/z): (M + H)<sup>+</sup>, calcd for C<sub>28</sub>H<sub>32</sub>FN<sub>7</sub>O<sub>2</sub>: 646.3175, found, 646.3196.

4.1.4. General procedure for the synthesis of **24a-g**

The synthetic methods of compounds **24a-g** are similarly to **23a-g**. The difference is that we need to replace the indole with 5-fluoroindole and the rest of the synthesis conditions are the same.

4.1.4.1. N-(2-((2-(dimethylamino)ethyl)(methyl)amino)-5-((4-(5-fluoro-1-methyl-1H-indol-3-yl)-6,6-dioxido-7,8-dihydro-5H-thiopyrano[4,3-d]pyrimidin-2-yl)amino)-4-methoxyphenyl)acrylamide (**24a**)

Light yellow solid. 35.8% yield, m.p: 254.4-256.7 °C. <sup>1</sup>H NMR (400 MHz, DMSO-*d*<sub>6</sub>) δ 9.74 (s, 1H, -CO-NH-), 9.13 (s, 1H, -NH-), 8.39 (s, 1H, indole-H), 8.24 (d, *J* = 4.0 Hz, 1H, indole-H), 7.76 (s, 1H, Ar-H), 7.53 (dt, *J* = 8.9, 4.4 Hz, 1H, indole-H), 7.42–7.33 (m, 1H, Ar-H), 7.08 (tt, *J* = 9.0, 4.1 Hz, 1H, indole-H), 6.99 (d, *J* = 7.6 Hz, 1H, -CH=CH<sub>2</sub>), 6.15 (d, *J* = 16.1 Hz, 1H, -CH=CH<sub>2</sub>), 5.64 (d, *J* = 9.2 Hz, 1H, -CH=CH<sub>2</sub>), 4.56 (s, 2H, -SO<sub>2</sub>-CH<sub>2</sub>-), 3.89 (s, 3H, -OCH<sub>3</sub>), 3.81 (s, 3H, indole-CH<sub>3</sub>), 3.62 (d, *J* = 6.6 Hz, 3H, -N-CH<sub>3</sub>), 3.38 (d, *J* = 6.5 Hz, 2H, -SO<sub>2</sub>-CH<sub>2</sub>-), 3.32 (s, 4H, -SO<sub>2</sub>-CH<sub>2</sub>-CH<sub>2</sub>-), -N-CH<sub>3</sub>-CH<sub>2</sub>-), 2.71 (d, *J* = 4.5 Hz, 6H, N-(CH<sub>3</sub>)<sub>2</sub>), 2.60 (s, 2H, -CH<sub>2</sub>-). <sup>13</sup>C NMR (400 MHz, DMSO-*d*<sub>6</sub>) δ 164.82, 159.93, 159.00, 157.92, 155.15, 147.07, 139.74, 135.01, 133.39, 127.96, 127.84, 127.25, 127.16, 126.84, 115.96, 111.88, 111.80, 109.40, 108.13, 104.98, 97.85, 57.71, 56.15, 53.42, 52.20, 48.79, 45.74, 45.71, 38.75, 32.73, 29.64. TOF MS ES<sup>+</sup> (m/z): (M + H)<sup>+</sup>, calcd for C<sub>28</sub>H<sub>32</sub>FN<sub>7</sub>O<sub>2</sub>: 622.2612, found, 622.2615.

4.1.4.2. 2-chloro-N-(2-((2-(dimethylamino)ethyl)(methyl)amino)-5-((4-(5-fluoro-1-methyl-1H-indol-3-yl)-6,6-dioxido-7,8-dihydro-5H-thiopyrano[4,3-d]pyrimidin-2-yl)amino)-4-methoxyphenyl)acrylamide (**24b**)

Light yellow solid. 32.9% yield, m.p: 259.8-261.4 °C. <sup>1</sup>H NMR (400 MHz, DMSO-*d*<sub>6</sub>) δ 10.02 (s, 1H, -CO-NH-), 9.32 (s,

1H, -NH-), 8.41 (s, 1H, indole-H), 8.31 (d,  $J = 3.9$  Hz, 1H, indole-H), 7.82 (s, 1H, Ar-H), 7.61 (dt,  $J = 8.8, 4.2$  Hz, 1H, indole-H), 7.44–7.35 (m, 1H, Ar-H), 7.08 (tt,  $J = 9.3, 4.0$  Hz, 1H, indole-H), 6.99 (d,  $J = 7.8$  Hz, 1H, -C=CH<sub>2</sub>), 5.79 (d,  $J = 8.8$  Hz, 1H, -C=CH<sub>2</sub>), 4.59 (s, 2H, -SO<sub>2</sub>-CH<sub>2</sub>-), 3.91 (s, 3H, -OCH<sub>3</sub>), 3.83 (s, 3H, indole-CH<sub>3</sub>), 3.64 (d,  $J = 6.2$  Hz, 3H, -N-CH<sub>3</sub>), 3.41 (d,  $J = 6.8$  Hz, 2H, -SO<sub>2</sub>-CH<sub>2</sub>-), 3.36 (s, 4H, -SO<sub>2</sub>-CH<sub>2</sub>-CH<sub>2</sub>-, -N-CH<sub>3</sub>-CH<sub>2</sub>-), 2.75 (d,  $J = 4.5$  Hz, 6H, N-(CH<sub>3</sub>)<sub>2</sub>), 2.61 (s, 2H, -CH<sub>2</sub>-). TOF MS ES<sup>+</sup> (m/z): (M + H)<sup>+</sup>, calcd for C<sub>28</sub>H<sub>32</sub>FN<sub>7</sub>O<sub>2</sub>: 656.2222, found, 656.2238.

4.1.4.3. (Z)-N-(2-((2-(dimethylamino)ethyl)(methylamino)-5-((4-(5-fluoro-1-methyl-1H-indol-3-yl)-6,6-dioxido-7,8-dihydro-5H-thiopyrano[4,3-d]pyrimidin-2-yl)amino)-4-methoxyphenyl)but-2-enamide (**24c**)

Light yellow solid. 35.6% yield, m.p: 257.9-259.4 °C. <sup>1</sup>H NMR (400 MHz, DMSO-*d*<sub>6</sub>) δ 9.83 (s, 1H, -CO-NH-), 8.89 (s, 1H, -NH-), 8.08 (d,  $J = 7.8$  Hz, 1H, indole-H), 7.93 (d,  $J = 8.3$  Hz, 1H, indole-H), 7.86 (d,  $J = 8.5$  Hz, 1H, indole-H), 7.18 (s, 1H, Ar-H), 7.09 (s, 1H, indole-H), 6.79 (s, 1H, Ar-H), 6.08 (s, 1H, -CO-CH=), 4.56 (s, 2H, -SO<sub>2</sub>-CH<sub>2</sub>-), 3.91 (s, 3H, -OCH<sub>3</sub>), 3.87 (s, 3H, indole-CH<sub>3</sub>), 3.77 (t,  $J = 6.9$  Hz, 3H, -N-CH<sub>3</sub>), 3.33 (t,  $J = 7.1$  Hz, 2H, -SO<sub>2</sub>-CH<sub>2</sub>-), 3.25–3.08 (m, 4H, -SO<sub>2</sub>-CH<sub>2</sub>-CH<sub>2</sub>-, -N-CH<sub>3</sub>-CH<sub>2</sub>-), 2.74 (s, 6H, N-(CH<sub>3</sub>)<sub>2</sub>), 2.63 (d,  $J = 13.1$  Hz, 2H, -CH<sub>2</sub>-), 2.52 (s, 3H, =C(CH<sub>3</sub>)<sub>2</sub>), 2.28 (s, 3H, =C(CH<sub>3</sub>)<sub>2</sub>). <sup>13</sup>C NMR (400 MHz, DMSO-*d*<sub>6</sub>) δ 166.31, 159.93, 159.28, 157.92, 155.12, 153.61, 147.07, 139.57, 135.04, 133.32, 128.21, 127.25, 126.84, 115.90, 115.25, 111.97, 111.80, 109.36, 107.89, 104.98, 97.79, 57.79, 56.15, 53.39, 52.15, 48.71, 45.74, 45.71, 38.75, 32.76, 29.61, 25.38, 20.76.

4.1.4.4. N-(2-((2-(dimethylamino)ethyl)(methylamino)-5-((4-(5-fluoro-1-methyl-1H-indol-3-yl)-6,6-dioxido-7,8-dihydro-5H-thiopyrano[4,3-d]pyrimidin-2-yl)amino)-4-methoxyphenyl)-3-methylbut-2-enamide (**24d**)

Light yellow solid. 33.9% yield, m.p: 258.1-260.7 °C. <sup>1</sup>H NMR (400 MHz, DMSO-*d*<sub>6</sub>) δ 9.86 (s, 1H, -CO-NH-), 8.48 (s, 1H, -NH-), 8.12 (s, 1H, indole-H), 7.83 (d,  $J = 9.9$  Hz, 1H, indole-H), 7.59 (d,  $J = 5.8$  Hz, 1H, indole-H), 7.49–7.34 (m, 1H, Ar-H), 7.30 (d,  $J = 8.4$  Hz, 1H, indole-H), 7.12 (t,  $J = 9.2$  Hz, 1H, =CH-CH<sub>3</sub>), 7.03 (s, 1H, Ar-H), 6.83 (d,  $J = 14.9$  Hz, 1H, -CO-CH=), 4.51 (s, 2H, -SO<sub>2</sub>-CH<sub>2</sub>-), 3.89 (s, 3H, -OCH<sub>3</sub>), 3.83 (s, 3H, indole-CH<sub>3</sub>), 3.63 (s, 2H, -N-CH<sub>3</sub>-CH<sub>2</sub>-), 3.36–3.24 (m, 4H, -SO<sub>2</sub>-CH<sub>2</sub>-CH<sub>2</sub>-), 2.71 (s, 3H, -N-CH<sub>3</sub>), 2.60 (s, 2H, -CH<sub>2</sub>-), 2.46 (s, 6H, N-(CH<sub>3</sub>)<sub>2</sub>), 2.38 (s, 3H, =CH-CH<sub>3</sub>). <sup>13</sup>C NMR (400 MHz, DMSO-*d*<sub>6</sub>) δ 165.19, 159.93, 159.44, 157.92, 155.19, 147.07, 141.01, 139.57, 135.11, 133.39, 128.14, 127.25, 126.84, 121.26, 115.89, 111.88, 111.80, 109.36, 107.92, 104.98, 97.85, 57.71, 56.15, 53.42, 52.15, 48.79, 45.74, 45.65, 38.75, 32.76, 29.59, 16.79. TOF MS ES<sup>+</sup> (m/z): (M + H)<sup>+</sup>, calcd for C<sub>28</sub>H<sub>32</sub>FN<sub>7</sub>O<sub>2</sub>: 650.2925, found, 650.2931.

4.1.4.5. (Z)-N-(2-((2-(dimethylamino)ethyl)(methylamino)-5-((4-(5-fluoro-1-methyl-1H-indol-3-yl)-6,6-dioxido-7,8-dihydro-5H-thiopyrano[4,3-d]pyrimidin-2-yl)amino)-4-methoxyphenyl)pent-2-enamide (**24e**)

Light yellow solid. 36.3% yield, m.p: 262.3.-263.5 °C. <sup>1</sup>H NMR (400 MHz, DMSO-*d*<sub>6</sub>) δ 9.49 (s, 1H, -CO-NH-), 8.39 (s, 1H, -NH-), 8.03 (s, 1H, indole-H), 7.79 (d,  $J = 10.3$  Hz, 1H, indole-H), 7.50 (d,  $J = 5.6$  Hz, 1H, indole-H), 7.42–7.32 (m,

1H, Ar-H), 7.26 (d,  $J = 8.5$  Hz, 1H, indole-H), 7.05 (t,  $J = 8.7$  Hz, 1H, =CH-CH<sub>2</sub>-), 6.96 (s, 1H, Ar-H), 6.78 (d,  $J = 15.3$  Hz, 1H, -CO-CH=), 4.48 (s, 2H, -SO<sub>2</sub>-CH<sub>2</sub>-), 3.87 (s, 3H, -OCH<sub>3</sub>), 3.82 (s, 3H, indole-CH<sub>3</sub>), 3.58 (s, 2H, -N-CH<sub>3</sub>-CH<sub>2</sub>-), 3.30–3.19 (m, 4H, -SO<sub>2</sub>-CH<sub>2</sub>-CH<sub>2</sub>-), 2.67 (s, 3H, -N-CH<sub>3</sub>), 2.59 (s, 2H, -CH<sub>2</sub>-), 2.48 (s, 6H, N-(CH<sub>3</sub>)<sub>2</sub>), 2.23–2.14 (m, 2H, -CH<sub>2</sub>-CH<sub>3</sub>), 1.04 (t,  $J = 7.6$  Hz, 3H, -CH<sub>2</sub>-CH<sub>3</sub>). TOF MS ES<sup>+</sup> (m/z): (M + H)<sup>+</sup>, calcd for C<sub>28</sub>H<sub>32</sub>FN<sub>7</sub>O<sub>2</sub>: 650.2925, found, 650.2928.

4.1.4.6. (Z)-N-(2-((2-(dimethylamino)ethyl)(methyl)amino)-5-((4-(5-fluoro-1-methyl-1H-indol-3-yl)-6,6-dioxido-7,8-dihydro-5H-thiopyrano[4,3-d]pyrimidin-2-yl)amino)-4-methoxyphenyl)-4-methylpent-2-enamide (**24f**)

Light yellow solid. 35.4% yield, m.p: 263.8-265.2 °C. <sup>1</sup>H NMR (400 MHz, DMSO-*d*<sub>6</sub>) δ 10.12 (s, 1H, -CO-NH-), 9.42 (s, 1H, -NH-), 8.37 (s, 1H, indole-H), 8.02 (s, 1H, Ar-H), 7.79 (d,  $J = 10.6$  Hz, 1H, indole-H), 7.50 (dd,  $J = 8.9, 4.6$  Hz, 1H, indole-H), 7.43–7.34 (m, 1H, indole-H), 7.07–7.01 (m, 1H, Ar-H), 6.95 (s, 1H, -CO-CH=), 6.73 (dd,  $J = 15.2, 6.2$  Hz, 1H, -CO-CH=CH), 4.48 (s, 2H, -SO<sub>2</sub>-CH<sub>2</sub>-), 3.87 (s, 3H, -OCH<sub>3</sub>), 3.83 (s, 3H, indole-CH<sub>3</sub>), 3.58 (t,  $J = 6.6$  Hz, 3H, -N-CH<sub>3</sub>), 3.27 (d,  $J = 5.4$  Hz, 6H, -N-CH<sub>3</sub>-CH<sub>2</sub>-, -SO<sub>2</sub>-CH<sub>2</sub>-CH<sub>2</sub>-), 2.73 (s, 6H, N-(CH<sub>3</sub>)<sub>2</sub>), 2.58 (s, 3H, -CH<sub>2</sub>-, -CH-(CH<sub>3</sub>)<sub>2</sub>), 1.04 (d,  $J = 6.7$  Hz, 6H, -CH-(CH<sub>3</sub>)<sub>2</sub>). <sup>13</sup>C NMR (400 MHz, DMSO-*d*<sub>6</sub>) δ 164.97, 160.28, 159.93, 157.92, 155.17, 147.07, 146.74, 139.55, 135.04, 133.32, 128.04, 127.25, 126.84, 121.90, 115.90, 112.41, 111.82, 109.36, 107.77, 104.98, 97.81, 57.77, 56.15, 53.42, 52.15, 48.71, 45.74, 45.71, 38.75, 32.76, 31.23, 29.60, 21.52, 21.46. TOF MS ES<sup>+</sup> (m/z): (M + H)<sup>+</sup>, calcd for C<sub>28</sub>H<sub>32</sub>FN<sub>7</sub>O<sub>2</sub>: 664.3081, found, 664.3088.

4.1.4.6. (Z)-N-(2-((2-(dimethylamino)ethyl)(methyl)amino)-5-((4-(5-fluoro-1-methyl-1H-indol-3-yl)-6,6-dioxido-7,8-dihydro-5H-thiopyrano[4,3-d]pyrimidin-2-yl)amino)-4-methoxyphenyl)hex-2-enamide (**24g**)

Light yellow solid. 30.8% yield, m.p: 264.4-266.8 °C. <sup>1</sup>H NMR (400 MHz, DMSO-*d*<sub>6</sub>) δ 9.60 (s, 1H, -CO-NH-), 8.48 (s, 1H, -NH-), 8.37 (s, 1H, indole-H), 8.02 (s, 1H, Ar-H), 7.78 (d,  $J = 10.5$  Hz, 1H, indole-H), 7.49 (dd,  $J = 8.9, 4.5$  Hz, 1H, indole-H), 7.43–7.32 (m, 1H, Ar-H), 7.04 (td,  $J = 9.0, 2.7$  Hz, 1H, indole-H), 6.97 (s, 1H, -CO-CH=CH-), 6.72 (dt,  $J = 14.5, 6.9$  Hz, 1H, -CO-CH=), 4.48 (s, 2H, -SO<sub>2</sub>-CH<sub>2</sub>-), 3.87 (s, 3H, -OCH<sub>3</sub>), 3.81 (s, 3H, indole-CH<sub>3</sub>), 3.58 (t,  $J = 6.7$  Hz, 3H, -N-CH<sub>3</sub>), 3.28 (t,  $J = 6.7$  Hz, 4H, N-CH<sub>3</sub>-CH<sub>2</sub>-, -SO<sub>2</sub>-CH<sub>2</sub>-), 3.11 (s, 2H, -SO<sub>2</sub>-CH<sub>2</sub>-CH<sub>2</sub>-), 2.62 (s, 2H, -CH<sub>2</sub>-), 2.54 (t,  $J = 10.4$  Hz, 8H, N-(CH<sub>3</sub>)<sub>2</sub>, -CH<sub>2</sub>-CH<sub>2</sub>-CH<sub>3</sub>), 1.48–1.43 (m, 2H, -CH<sub>2</sub>-CH<sub>2</sub>-CH<sub>3</sub>), 0.90 (t,  $J = 7.3$  Hz, 3H, -CH<sub>2</sub>-CH<sub>2</sub>-CH<sub>3</sub>). TOF MS ES<sup>+</sup> (m/z): (M + H)<sup>+</sup>, calcd for C<sub>28</sub>H<sub>32</sub>FN<sub>7</sub>O<sub>2</sub>: 664.3081, found, 664.3085.

#### 4.2 Molecular docking study

The Sybyl 8.1 software packages (TRIPOS Associates Inc., USA) were applied to carry out the molecular docking simulation. All the docking approaches used in the experiment can be found in the Tripos bookshelf. The crystal structure of EGFR-T790M (PDB code: 3IKA) used in the docking were downloaded from the website <http://www.rcsb.org/>. The protein preparation procedures implemented by using the Structure Preparation Tool in Sybyl, mainly including fixing the

residues, removing hetero-atoms and water molecules, adding hydrogen atoms and optimizing the whole structure of the reconstruction protein, etc. The inhibitor 3 was first removed from the EGFR-T790M crystal structure. Then the target compounds were put into the binding site. The surflex-dock algorithm was used to calculate the energy values between the ligands and protein. Only the best-scoring complex was used for the further binding site analysis. The Pymol 1.8x (<https://pymol.org>). software was used to modify and process the final docking results.

### 4.3. 3D-QSAR on HeLa cell line

#### 4.3.1. Data set

In this research, in order to further investigate the antiproliferative activity of target compounds against HeLa cells, the in vitro antiproliferative activity data of HeLa cells were chosen to construct the 3D-Quantitative Structure Activity Relationship (3D-QSAR) models. **Table 4** listed the structures of all target compounds and the IC<sub>50</sub> values against HeLa cell. CoMFA and CoMSIA analysis were performed using IC<sub>50</sub> values for all target compounds against HeLa cells. Then, the IC<sub>50</sub> values were converted to pIC<sub>50</sub> values according to the following formula:

$$pIC_{50} = \lg \frac{1}{IC_{50}}$$

#### 4.3.2. Structure optimization

Construction of all target compounds, structural optimization, and 3D-QSAR modeling were all performed on Sybyl 8.1 (Tripos Associates Inc.) software. The Tripos force field and conjugate gradient method were used to minimize the structure of all target compounds. The target charge was set to the Gasteiger-hückler charge. The convergence criterion was 0.05 kcal/(mol·Å), and the maximum optimization frequency was 10000. Subsequently, Compound **23g** with the highest pIC<sub>50</sub> value was chosen as the template molecule, and the skeleton N<sub>1</sub>-(7,8-dihydro-5H-thiopyrano[4,3-d]pyrimidin-2-yl) benzene-1,3-diamine was set as alignment template to carry out molecular superposition.

#### 4.3.3. CoMFA and CoMSIA studies

3D-QSAR analyses of target compounds were performed using the Sybyl 8.1 software default settings. Steric and electrostatic fields energy (CoMFA mode) were calculated using a positively charged SP<sup>3</sup> hybridization C atom with a van der Waals force radius of 1.52 Å as the probe atom (default probe atom in Sybyl). The interaction energy values between C atom and target compounds were calculated by calculating the interaction energy values of C atom and compounds according to the Lennard-Jones and Coulomb potential energy functions with the threshold value of 30 KJ/mol.

According to the Lennard-Jones and Coulomb potential energy functions. The electrostatic field energy and the steric field energy around the target compound were determined. The threshold was set to 30 kcal/mol. CoMSIA model

used Gaussian function as the main optimization algorithm. This method can minimize data fluctuations caused by sharp changes in the potential energy of the molecular surface. In addition, in order to compensate for the shortcomings of the CoMFA model, the CoMSIA model also added hydrophobic field, donor and acceptor field.

Both CoMFA and CoMSIA models were used partial least squares (PLS) regression analysis to perform energy analysis of various fields. The "Leave-One-Out" mode was used for cross-validation analysis to obtain the optimal principal component number  $N$  and the cross-validation coefficient  $q^2$ , which mainly reflect the prediction ability of the current model. Finally, CoMFA and CoMSIA models of the target compounds were established and the corresponding contour maps were displayed<sup>30,32</sup>. The cross-validated coefficient  $q^2$  (or  $r^2$ ) was evaluated as:

$$q^2 = 1 - \frac{\sum(Y_{pred} - Y_{exp})^2}{\sum(Y_{exp} - Y_{mean})^2}$$

The values of  $Y_{pred}$ ,  $Y_{exp}$ ,  $Y_{mean}$  represent the  $pIC_{50}$  of the predicted, experimental, and mean values, respectively.

The standard error of estimate SE and the Fisher test F value were also derived to evaluate the predictive quality of the models.

#### 4.4 *In vitro enzymatic activity assay*

The mobility shift assay was applied to test the activity for the target compounds against EGFR<sup>WT</sup> and EGFR<sup>T790M/L858R</sup> kinases. The kinase activity test was determined with enzyme-linked immunosorbent assay (ELISA). The detailed experimental operation can be found in our previous research<sup>33</sup>.

#### 4.5 *In vitro antiproliferative activity assay*

Hela, A549 and H1975 cell were obtained from the Cell Cultures Collection of Chinese Academy of Sciences (Shanghai Institutes for Biological Sciences, Chinese Academy of Sciences). All the cancer cells were treated with different concentrations of the target compounds, and then cultured and propagated in 96-well plates for 72 h. The MTT assay was used to test the in vitro antiproliferative activities of target compounds over Hela, A549 and H1975 cancer cells, with the EGFR inhibitor AZD9291 as positive control. The results expressed as  $IC_{50}$  (half-maximal inhibitory concentration) and all the  $IC_{50}$  values were the averages of three determinations and calculated by using the Bacus Laboratories Incorporated Slide Scanner (Bliss) software. The detailed experimental operation can be found in our previous research<sup>33</sup>.

#### 4.6 *Cell cycle progression assay*

A549 cells were seeded and incubated in a 6-well plate for 24 h. Next, the A549 cells were treated with 0.1% dimethyl sulfoxide (vehicle group), **22b** and **23g** for 24 hours, respectively. Cells were collected and prepared as monolayer cell suspensions. After fixation with 70% ice-cold ethanol for 12 h, the fluorochrome PI was added into the monolayer cell

suspensions and incubated for the specified time. The DNA contents were measured by FACS Calibur flow cytometer (B. D. Accuri C6, BD Biosciences, USA). The detailed experimental operation can be found in our previous research<sup>33</sup>.

#### 4.7 Cell apoptosis assay

A549 cells were seeded and incubated in a 6-well plate for 24 h. Next, the A549 cells were treated with 0.1% dimethyl sulfoxide (vehicle group), **22b** and **23g** for 24 hours, respectively. Cells were collected and prepared as monolayer cell suspensions. Finally, the fluorochrome PI and Annexin V-FITC were added into the monolayer cell suspensions and incubated for the specified time. The results analyzed by FACS Calibur flow cytometer (B. D. Accuri C6, BD Biosciences, USA) using Cell Quest software.

#### 4.8 Western blot analysis

Hela cells were treated with positive control AZD9291 or different concentration of **23g** for 24 h. The whole cell proteins were extracted by RIPA lysis buffer. The concentration of the cell lysates was measured by Bio-Rad (California, USA) BCA Pro-tein Quantitation Assay Kit (California, USA). The Equal amount of protein was subjected to 10% SDS polyacrylamide gel electrophoresis and then transferred to PVDF membrane under ice bath conditions. Next, the PVDF membranes were incubated with different protein of target proteins (EGFR, p-EGFR, GAPDH). Finally, exposure development was carried out with film in a dark room. The density of the bands were analyzed by Image Lab software (Molecular Dynamics, Sunnyvale, CA, USA), and then expressed as the percentage of the density of the GAPDH band.

## 5. Acknowledgements

We gratefully acknowledge the generous support provided by The National Natural Science Funds of China (No. 21662014 and 81860692), Jiangxi Outstanding Youth Talent Support Program (20171BCB23078), Natural Science Foundation of Jiangxi, China (20171ACB21052, 20181BBG70003, 20181ACB20025), Jiangxi Science and Technology Normal University Innovative Research Team (2017CXTD002).

## 6. References

1. Tiseo M, Bartolotti M, Gelsomino F, *et al.* Emerging role of gefitinib in the treatment of non-small-cell lung cancer (NSCLC). *Drug Des Dev Ther*, 2010;4:81-98.
2. Ren YY, Yao YB, Ma Q, Zhong DS. EGFR gene-mutation status correlated with therapeutic decision making in lung adenocarcinoma. *Oncotargets Ther* 2015;8:3017-3020.
3. Tu YB, Wang CL, Yang ZH, Zhao BB, Lai LG, Yang Q, *et al.* Discovery of novel quinazoline derivatives bearing semicarbazone moiety as potent EGFR kinase inhibitors. *Comput Struct Biotec* 2018;16:462-478.

4. Jiang B, Liu L. PI3K/PTEN signaling in angiogenesis and tumorigenesis. *Adv Cancer Res* 2009;1:19-65.
5. Courtney KD, Corcoran RB, Engelman JA. The PI3K Pathway As drug target in human cancer. *J Clin Oncol* 2010;8:1075-1083.
6. Vivanco I, Sawyers CL. The phosphatidylinositol 3-Kinase AKT pathway in human cancer. *Nat Rev Cancer* 2002;7:489-501.
7. OuYang YQ, Wang CL, Zhao BB, Xiong HH, Xiao Z, Zhang BL, et al. Design, synthesis, antiproliferative activity and docking studies of quinazoline derivatives bearing oxazole or imidazole as potential EGFR inhibitors. *New J Chem* 2018;42:17203-17215.
8. Marchetti A, Martella C, Felicioni L, Barassi F, Salvatore S, Chella A, et al. EGFR mutations in non-small-cell lung cancer: analysis of a large series of cases and development of a rapid and sensitive method for diagnostic screening with potential implications on pharmacologic treatment. *J Clin Oncol* 2005;4:857-865.
9. Gschwind A, Fischer OM, Ullrich A. The discovery of receptor tyrosine kinases: targets for cancer therapy. *Nat Revs Cancer* 2004;5:361-370.
10. Chico LK, Van Eldik LJ, Watterson DM. Targeting protein kinases in central nervous system disorders. *Nat Rev Drug Discov* 2009;11:892-909.
11. Torre LA, Bray F, Siegel RL, Ferlay S, Lortet-Tieulent J, Jemal A. Global cancer statistics, 2012. *Ca Cancer J Clin* 2015;2:87-108.
12. Ciardiello F, Tortora G. A novel approach in the treatment of cancer: targeting the epidermal growth factor receptor. *Clin Cancer Res* 2001;10:2958-2970.
13. Tu YB, Wang CL, Xu S, Lan Z, Li W, Han JQ, et al. Design, synthesis, and docking studies of quinazoline analogues bearing aryl semicarbazone scaffolds as potent EGFR inhibitors. *Bioorgan Med Chem* 2017;12:3148-3157.
14. Rosell R, Molina MA, Costa C, Simonetti S, Gimenez-Capitan A, Bertran-Alamillo J, et al. Pretreatment EGFR T790M mutation and BRCA1 mRNA expression in erlotinib-treated advanced non-small-cell lung cancer patients with EGFR mutations. *Clin Cancer Res* 2011;5:1160-1168.
15. Yang SY, Yang TY, Chen KC, Li YJ, Hus KH, Tsai CR, et al. EGFR L858R mutation and polymorphisms of genes related to estrogen biosynthesis and metabolism in never-smoking female lung adenocarcinoma patients. *Clin Cancer Res* 2011;8:2149-2158.
16. Thress KS, Paweletz CP, Felip E, Cho BC, Stetson D, Dougherty B, et al. Acquired EGFR C797S mediates resistance to AZD9291 in advanced non-small cell lung cancer harboring EGFR T790M. *Nat Med*

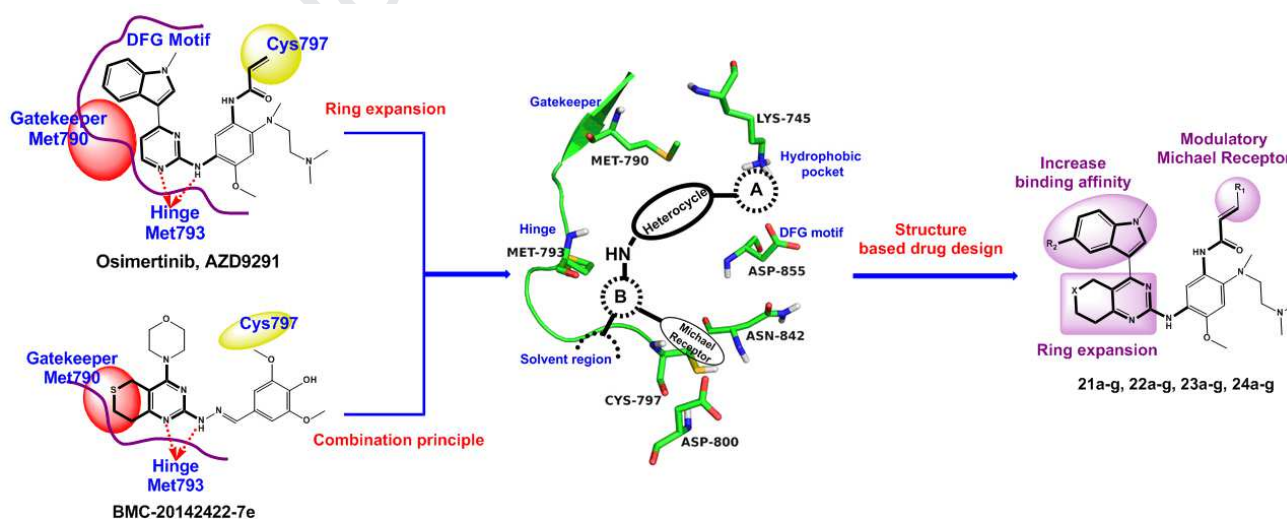
2015;6:560-562.

17. Eberlein CA , Stetson D , Markovets AA , Al-Kadhimi KJ, Lai Z, Fisher PR, et al. Acquired resistance to mutant-selective EGFR inhibitor AZD9291 is associated with increased dependence on RAS signaling in preclinical models. *Cancer Res* 2015;12:2489-2500.
18. Kris MG, Natale RB, Herbst RS, Lynch TJ, Prager D, Belani CP, et al. Efficacy of gefitinib, an inhibitor of the epidermal growth factor receptor tyrosine kinase, in symptomatic patients with non-small cell lung cancer: a randomized trial. *JAMA* 2003;16:2149-2158.
19. Solca F, Dahl G, Zoephel A, Bader G, Sanderson M, Klein C, et al. Target binding properties and cellular activity of afatinib (BIBW 2992), an irreversible ErbB family blocker. *J Pharmacol Exp Ther* 2012;2:342-350.
20. Finlay MR, Anderton M, Ashton S, Ballard P, Bethel P, Box MR, et al. Discovery of a potent and selective EGFR inhibitor (AZD9291) of both sensitizing and T790M resistance mutations that spares the wild type form of the receptor. *J Med Chem* 2014;20:8249-8267.
21. Cross DA, Ashton SE, Ghiorghiu S, Eberlein C, Nebhan CA, Spitzler PJ, et al. AZD9291, an irreversible EGFR TKI, overcomes T790M-mediated resistance to EGFR inhibitors in lung cancer. *Cancer Discov* 2014;9:1046-1061.
22. Oxnard GR, Thress KS, Alden RS, Lawrance R, Paweletz CP, Cantarini M, et al. Association between plasma genotyping and outcomes of treatment with osimertinib (AZD9291) in advanced non-small-cell lung cancer. *J Clin Oncol* 2016; 28:3375-3382.
23. Hussain SP, Hofseth LJ, Harris CC. Radical causes of cancer. *Nat Rev Cancer* 2003;4:276-285.
24. Zanagnolo V, Minig LA, Gadducci A, Maggino T, Sartori E, Zola P, et al. Surveillance procedures for patients for cervical carcinoma: a review of the literature. *Int J Gynecol Cancer* 2009;2:194-201.
25. Roden R, Wu TC. How will HPV vaccines affect cervical cancer? *Nat Rev Cancer* 2006;10:753-763.
26. Zhu WF, Sun CY, Xu S, Wu Cj, Wu JL, Xu MZ, et al. Design, synthesis, anticancer activity and docking studies of novel 4-morpholino-7, 8-dihydro-5H-thiopyrano [4, 3-d] pyrimidine derivatives as mTOR inhibitors. *Bioorgan Med Chem* 2014;24: 6746-6754.
27. Junttila TT, Akita RW, Parsons K, Fields C, Phillips GD, Friedman LS, et al. Ligand-independent HER2/HER3/PI3K complex is disrupted by trastuzumab and is effectively inhibited by the PI3K inhibitor GDC-0941. *Cancer Cell* 2009;5:429-440.
28. Liu KK, Bailey S, Dinh DM, Lam H, Li C, Wells PA, et al. Conformationally-restricted cyclic sulfones as potent and selective mTOR kinase inhibitors. *Bioorg Med Chem Lett* 2012;15:5114-5117.
29. Cao R, Guan X, Shi B, Chen ZY, Ren ZH, Peng WL, et al. Design, synthesis and 3D-QSAR of  $\beta$ -carboline

derivatives as potent antitumor agents. *Eur J Med Chem* 2010;6:2503-2515.

30. Politi A, Durdagi S, Moutevelis P, Kokotos G, Papadopoulos MG, Mavromoustakos T, et al. Application of 3D QSAR CoMFA/CoMSIA and in silico docking studies on novel renin inhibitors against cardiovascular diseases. *Eur J Med Chem* 2009;9:3703-3711.
31. Shaw AY, Chang CY, Hsu MY, Lu PJ, Yang CN, Chen HL, et al. Synthesis and structure-activity relationship study of 8-hydroxyquinoline-derived Mannich bases as anticancer agents. *Eur J Med Chem* 2010;7:2860-2867.
32. Zhu WF, Liu YJ, Zhai X, Wang X, Zhu Y, Wu D, et al. Design, synthesis and 3D-QSAR analysis of novel 2-hydrazinyl-4-morpholinthieno [3, 2-d] pyrimidine derivatives as potential antitumor agents. *Eur J Med Chem* 2012;57:162-175.
33. Zhao BB, Xiao Z, Qi JG, Luo R, Lan Z, Zhang YZ, et al. Design, synthesis and biological evaluation of AZD9291 derivatives as selective and potent EGFR<sup>L858R/T790M</sup> inhibitors. *Eur J Med Chem* 2019;1:367-380.
34. Sun CY, Chen C, Xu S, Wang JQ, Zhu Y, Kong DJ, et al. Synthesis and anticancer activity of novel 4-morpholino-7,8-dihydro-5H-thiopyrano[4,3-d]pyrimidine derivatives bearing chromone moiety. *Bioorgan Med Chem* 2016;24: 3862-3869.
35. Butterworth S, Finlay MR, Ward RA, Kadambar VK, Chandrashekar RC, Murugan A, et al. 2-(2,4,5-Substituted-anilino) pyrimidine derivatives as EGFR modulators useful for treating cancer. WO201314448A1, 2013-01-31.

## Table of Contents



Four series of AZ9291 derivatives bearing thiopyranopyrimidine structure were designed, synthesized. The potent compound **23g** exhibited more than 125-fold selectivity against EGFR<sup>L858R/T790M</sup> double mutations. Furthermore, compound **23g** also inhibited A549 cells, Hela cells and H1975 cells proliferation at a low concentration, and the IC<sub>50</sub> values were 0.057 μM, 0.104 μM and 0.916 μM, respectively.

Journal Pre-proof

## Research Highlights

- Four series of potent and selective EGFR<sup>L858R/T790M</sup> inhibitors were designed and characterized.
- The selectivity of **23g** against wild-type EGFR was near to 125-fold.
- **20g** also inhibited A549 cells, Hela cells and H1975 cells proliferation at a low concentration, and the IC<sub>50</sub> values were 0.057  $\mu$ M, 0.104  $\mu$ M and 0.916  $\mu$ M, respectively.
- 3D-QSAR analysis employed by CoMFA and CoMSIA model on Hela cell line was investigated.